

The Pennsylvania State University

The Graduate School

College of Engineering

**POLY(3,4-ETHYLENE DIOXYTHIOPHENE) NANOFIBERS  
FOR NEURAL INTERFACES**

A Thesis in

Bioengineering

by

Kelly Layton Kampstra

© Kelly Layton Kampstra

Submitted in Partial Fulfillment  
of the Requirements  
for the Degree of

Master of Science

August 2014

The thesis of Kelly Layton Kampstra was reviewed and approved\* by the following:

Mohammad Reza Abidian  
Assistant Professor of Biomedical Engineering  
Thesis Advisor

Sheereen Majd  
Assistant Professor of Biomedical Engineering

Siyang Zheng  
Assistant Professor of Biomedical Engineering

William Hancock  
Professor of Biomedical Engineering  
Graduate Program Officer

\*Signatures are on file in the Graduate School.

## ABSTRACT

The ability to directly interface with the nervous system is necessary to better understand the function of this complex system and to gain insight into new methods to treat neural injury and disease. Further, the materials used at the biotic-abiotic interface are critical to the functionality of such therapies. Conducting polymers have shown promise for use in neural interfacing for several reasons: their electrical conductivity, the ability to incorporate and release biomolecules, and the ease of fabricating nano-scale morphologies. Conducting polymers such as polypyrrole and poly(3,4-ethylene dioxythiophene) have been used in applications such as drug delivery, biosensing, neural recording, and tissue engineering. This research focused on developing conducting polymer nanofibers for use in such applications.

The first part of this research was the development of a sensitive biosensor using conducting polymer nanofibers. Sensors are fabricated on microelectrodes coated with conducting polymer films or nanofibers with the enzyme glucose oxidase incorporated. The conducting polymer nanofibers were shown to incorporate a larger amount of the enzyme and to have lower impedance than the conducting polymer films. In turn, the nanofibers had a higher sensitivity to glucose than the films and also retained a larger percentage of that sensitivity over time. Finally, the nanofibers showed less of a loss in charge storage capacity over time, which was further enhanced by the use of lower polarization potentials. These biosensors serve as a proof of concept such sensor design in the detection of other neurochemicals and neurotransmitters.

The second part of this research was the fabrication and characterization of conductive hydrogel nanofibers using a method that does not require a hard metal substrate. Nanofibers were fabricated from a blend of varying amounts of conducting polymer nanoparticles and hydrogel. The morphology, swelling ratio, and electrical impedance of such nanofibers were measured and compared to films of similar material. Increasing amounts of conducting polymer nanoparticles led to reduced swelling ratios and larger reductions in impedance. Additionally, the film and nanofiber morphologies had distinctly different impedance spectra in the low frequency ranges. Such conductive hydrogel nanofibers could find future application in drug delivery or neural tissue engineering.

# TABLE OF CONTENTS

List of Tables .....	v
List of Figures .....	vi
List of Abbreviations.....	viii
Acknowledgements.....	ix
Chapter 1. Introduction.....	1
1.1 Materials for Neural Interfaces.....	1
1.2 Conducting Polymers in Neural Interfaces .....	3
1.3 Electrospinning in Biomedical Applications .....	7
1.4 Conducting Polymer – Hydrogel Blends .....	9
Chapter 2. Conducting Polymer Nanofibers for Sensitive Detection of Glucose.....	11
2.1 Materials & Methods .....	13
2.2 Results & Discussion .....	14
2.3 Conclusion.....	25
Chapter 3. Conducting Polymer – Hydrogel Nanofibers .....	27
3.1 Materials & Methods .....	28
3.2 Results & Discussion .....	29
3.3 Conclusion.....	34
Chapter 4. Conclusion & Future Direction.....	35
Bibliography .....	36

## LIST OF TABLES

**Table 1.** Swelling ratio of PEDOT:PSS - PEO films and nanofibers made from solutions containing 0%, 15%, 20%, or 25% PEDOT:PSS. (Page 32)

## LIST OF FIGURES

- Figure 1.** Schematic of chronic response to implantation of neural material (Fattahi, Yang et al. 2014). Figure adapted from Fattahi et. al. with permission of John Wiley & Sons. (Page 2)
- Figure 2.** Chemical structures of several conducting polymers (Guimard, Gomez et al. 2007). Figure reproduced from Guimard et. al. with permission of Elsevier. (Page 4)
- Figure 3.** Mechanism of electrochemical polymerization initiated by oxidation of monomer at working electrode (Guimard, Gomez et al. 2007). Figure reproduced from Guimard et. al. with permission of Elsevier. (Page 5)
- Figure 4.** Electrospinning is a fabrication method that uses high voltages to spray a polymer solution onto a stationary target where it is collected as a random fiber mat or onto a rotating wheel where it is collected as aligned fibers (Greiner and Wendorff 2007). Figure reproduced from Greiner et. al. with permission of John Wiley & Sons. (Page 7)
- Figure 5.** Fabrication of conducting polymer-hydrogel blend by electropolymerization of conducting polymer within a polymerized hydrogel. (Page 9)
- Figure 6.** Schematic illustration PEDOT film + GOx coated microelectrodes. SEM image of PEDOT film and PEDOT nanofibers on neural electrode. (Page 15)
- Figure 7.** Schematic illustration of fabrication process of PEDOT nanofibers showing electrospinning of PLLA template fibers followed by electrodeposition of PEDOT around the fibers at electrode site (Abidian, Kim et al. 2006). Optical images are representative of the fabrication process. Figure adapted from Abidian et. al. with permission of John Wiley & Sons. (Page 15)
- Figure 8.** Schematic illustration image of PEDOT nanofiber + GOx. SEM image representative of PEDOT nanofibers. (Page 16)
- Figure 9.** FTIR spectrum of PEDOT nanofibers with and without GOx. (Page 17)
- Figure 10.** EQCM showing significantly more GOx incorporated into PEDOT nanofiber + GOx sensors compared to PEDOT film + GOx sensors. (Page 18)
- Figure 11.** Impedance spectrum of bare platinum electrode sites compared to sites with PEDOT + GOx film and PEDOT + GOx nanofibers. (Page 19)

- Figure 12.** Amperometric response of PEDOT film + GOx and PEDOT nanofiber + GOx to serial injections of glucose at +300 mV (A) and + 700 mV (B). (Page 20)
- Figure 13.** Amperometric response curves of PEDOT + GOx films and PEDOT + GOx nanofiber sensors at + 300 mV and + 700 mV polarization potentials. (Page 21)
- Figure 14.** Sensitivity of PEDOT film + GOx sensors and PEDOT nanofiber + GOx sensors at +300 mV and +700 mV polarization potentials at Day 1 and Day 30. (Page 22)
- Figure 15.** Sensitivity of PEDOT film + GOx and PEDOT nanofiber + GOx sensors at +300 mV and +700 mV over the course of 30 days. (Page 24)
- Figure 16.** Charge storage capacity (CSC) of PEDOT film + GOx and PEDOT nanofiber + GOx at +300 mV and +700 mV potential over 280 minutes of CV. (Page 25)
- Figure 17.** SEM images of electrospun nanofibers of 0% PEDOT:PSS – PEO (B), 15% PEDOT:PSS – PEO (A,C), and 25% PEDOT:PSS – PEO (D) showing randomly oriented mats of nanofibers and similar nanofiber morphology for each PEDOT:PSS concentration. 20% PEDOT:PSS – PEO nanofibers had similar morphology (not shown). (Page 30)
- Figure 18.** Diameter of PEDOT:PSS – PEO nanofibers by PEDOT:PSS content. (Page 30)
- Figure 19.** EDS spectra obtained for a mat of PEDOT:PSS – PEO nanofibers fabricated from a solution containing 0% PEDOT:PSS or 25% PEDOT:PSS. The sulfur peak indicated the presence of PEDOT:PSS nanoparticles within the 25% PEDOT:PSS nanofibers that is absent in the 0% PEDOT:PSS nanofibers. (Page 31)
- Figure 20.** Reduction in impedance at 10 Hz in PEDOT:PSS – PEO film and PEDOT:PSS – PEO nanofiber samples. (Page 33)
- Figure 21.** Impedance spectra for 0% PEDOT:PSS – PEO samples (A) and 25% PEDOT:PSS – PEO samples (B). (Page 34)

## LIST OF ABBREVIATIONS

A – Amp	M – molar
AC – alternating current	M – mega-
Ag/AgCl – silver/silver chloride	m – milli-
ANOVA – analysis of variance	m – meter
BDNF – brain derived nerve growth factor	M.W. – molecular weight
C – Coulomb	NGF – nerve growth factor
$C_f$ – sensitivity factor	n – nano-
$Ca^{+2}$ – calcium ion	Pa - Pascals
cm – centimeter	PBS – phosphate buffered saline
CNS – central nervous system	PEDOT - poly(3,4-ethylenedioxythiophene)
CNT – carbon nanotube	PEO – polyethylene oxide
CSC – charge storage capacity	PETA - pentaerythritol triacrylate
Cu - copper	PLLA – poly(L-lactide)
CV – cyclic voltammetry	PPy – polypyrrole
d – deci -	Pt – platinum
DBS - dodecylbenzenesulfonate	S – seimen
DI – deionized	s – second
EDS – energy dispersive spectroscopy	SEM – scanning electron microscopy
EQCM – electrochemical quartz crystal microbalance	TEM – transmission electron microscopy
eV – electron volt	TiO <sub>2</sub> – titanium dioxide
FTIR – fourier transform infrared spectroscopy	V – volt
GOx – glucose oxidase	W – tungsten
g – gram	W – watt
hr – hour	w/v – weight per volume
Hz – hertz	°C – degrees Celsius
k – kilo -	$\Delta f$ – change in frequency
L – liter	$\Delta m$ – change in mass
	$\mu$ - micro-
	$\Omega$ – ohm

## **ACKNOWLEDGEMENTS**

I would like to express my gratitude to my thesis advisor Prof. Mohammad Reza Abidian for his support and guidance throughout my graduate studies. Also, I would like to thank Guang Yang for his contribution to this work in completing the FTIR, EQCM, and cyclic voltammetry studies. Finally, I appreciate the time and feedback given by my committee members Prof. Sheereen Majd and Prof. Siyang Zheng.

# Chapter 1. INTRODUCTION

## 1.1 Materials for Neural Interfaces

The ability to interface man-made devices with the nervous system provides the opportunity to first better understand the complex function of this system and to then develop improved technologies and therapies to treat injuries and diseases within the nervous system. People with conditions such as paralysis, Parkinson's disease, Alzheimer's disease, epilepsy, and deafness could benefit from improved neural interfacing that spans a range of functionality. For example, a microarray of silicon electrodes implanted in the primary motor cortex has been used to control prosthetic devices for a human with tetraplegia (Hochberg, Bacher et al. 2012) while degradable polymers have been used as scaffolds for neural stem cells that adhere, differentiate, and migrate into hypoxic-ischemic cavities within the brain (Park, Teng et al. 2002).

Historically, neural interfacing has focused on electrical recording and stimulation using conventional electronic materials; however, application of other materials can not only enhance recording and stimulation, but also improve the material's interaction with neural tissue. Conventional electronic materials are inorganic metals, which are hard, dry, and static in nature, making them less than ideal for interfacing with neural tissue, which is soft, wet, and dynamic (Fattahi, Yang et al. 2014).

The implantation of a foreign material within neural tissue leads to an acute and chronic immune response. Within the central nervous system (CNS), acute inflammation occurs following mechanical trauma such as electrode insertion. This inflammation causes edema and activation of immune cells such as microglia, both of which cause neighboring tissue to be pushed away, and initially very few neurons can be found within 100 $\mu$ m of the material. Following this initial response, a chronic reaction to the implanted material will take place as reactive astrocytes, activated microglia, macrophages, and fibroblasts form a glial scar that isolates the material from the living tissue (**Figure 1**) (Silver and Miller 2004; Fattahi, Yang et al. 2014). In addition to creating a physical barrier between the material and the neural tissue, such glial scars also produce chemical factors that inhibit the growth of neural processes (Yiu and He 2006). Minimizing this immune response is important in order for the material to fully integrate with the surrounding tissue.

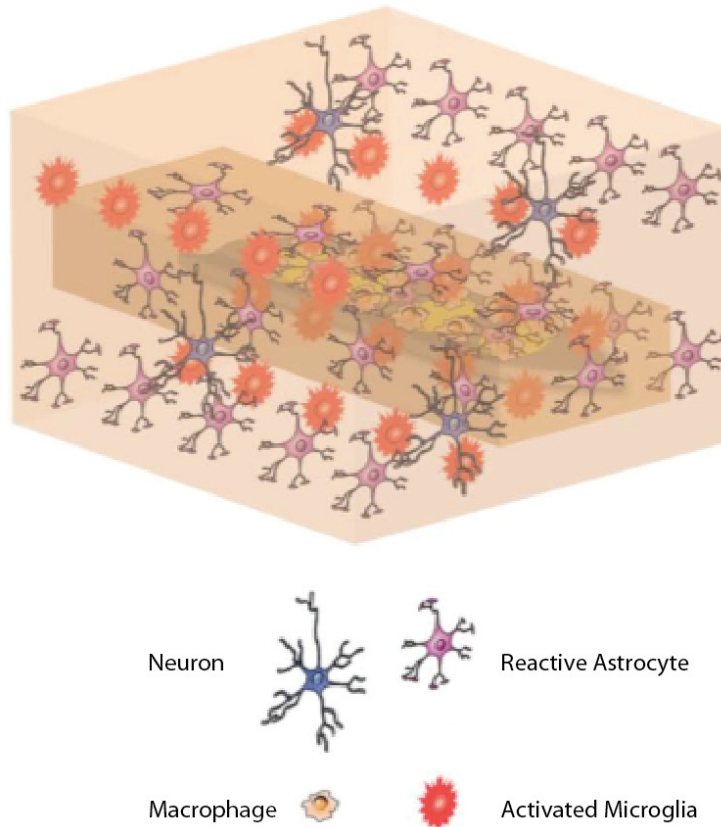


**Figure 1.** Schematic of chronic response to implantation of neural material (Fattahi, Yang et al. 2014). Figure adapted from Fattahi et. al. with permission of John Wiley & Sons.

Chemical, physical, and mechanical properties of the implanted material are important factors in modulating the chronic tissue response and enhancing neuron interaction with the material. To mimic neural tissue and cause minimal inflammation and neuronal cell loss, neural interface materials should be electroactive, have soft mechanical properties, have nanoscale structural features, and incorporate bioactive molecules to improve biocompatibility. Studies suggest that physical characteristics can modulate the acute tissue response while surface modification with bioactive molecules can modulate the chronic tissue response (Fattahi, Yang et al. 2014). Physical characteristics such as electrode size, geometry, and surface roughness have been modified with the goal of minimizing tissue response (Szarowski, Andersen et al. 2003; Karumbaiah, Saxena et al. 2013). Additionally, mechanical properties of interface materials have been shown to affect neurite extension. Materials with elastic moduli similar to the axonal growth cones have been shown to enhance neurite outgrowth while materials with elastic moduli greater than the axonal growth cone are correlated with adhesion site detachment and neurite retraction (Franze and Guck 2010).

In addition to physical and mechanical properties, materials with nanoscale structural features can mimic elements of neurons, glial cells, and extracellular matrix and thus improve integration between the material and the neural tissue (Silva 2006). Cells in the nervous system naturally migrate along tracts of glial cells or oriented extracellular matrix fibers. For example during the histogenesis of the cerebral cortex, cortical neurons are guided along radial glial cells (Hoffman-Kim, Mitchel et al. 2010). Such contact guidance is also seen following nerve transection in the peripheral nervous system in which Schwann cells lay down tracks and produce growth factors to aid in the axon regeneration (Hoffman-Kim, Mitchel et al. 2010). Similar responses have been observed using engineered materials. For example, aligned polymer microfibers could orient and increase neurite outgrowth thereby enhancing axonal regeneration in rats with complete spinal cord transection (Hurtado, Cregg et al. 2011).

Finally, the incorporation of bioactive molecules in neural interface materials can modulate the inflammatory response and improve biocompatibility. Studies of surface modification with anti-inflammatory compounds, adhesion proteins, or growth factors have been completed with promising results (Dodla and Bellamkonda 2008; Kim, Caldwell et al. 2009). Materials capable of release of drugs or growth factors could be used to fight infection or promote neurite outgrowth (Green, Lovell et al. 2008). For example, silicone tubes coated with laminin and fibronectin have been used to improve the axonal regeneration over a sciatic nerve gap and neurotrophic factors such as nerve growth factor (NGF) and brain-derived nerve growth factor (BDNF) that were released from degradable polymer matrices promoted survival and outgrowth of neurons (Schmidt and Leach 2003).

## **1.2 Conducting Polymers in Neural Interfaces**

Conducting polymers consist of organic chains of alternating double and single-bonded  $sp^2$  hybridized atoms with their p-orbitals overlapped (**Figure 2**). These conjugated bonds allow for delocalized electrons and charge mobility along the polymer backbone, which endows conductivity to the polymer when doped with charge carriers. Doping involves oxidizing or reducing the neutral polymer in the presence of a counter anion or cation respectively, resulting in a neutral system of a charged conducting polymer backbone with closely associated counter ions. Conductivity of these polymers can vary greatly depending on the doping and can be upwards of  $10^3$  S/cm (MacDiarmid 2001; Guimard, Gomez et al.

2007). In addition, their response to electrochemical oxidation and reduction can produce a wide range of wettability, color, and volume (Fattahi, Yang et al. 2014).

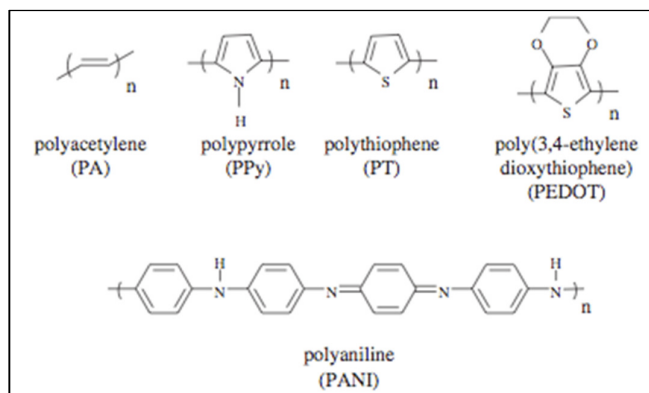


**Figure 2.** Chemical structures of several conducting polymers (Guimard, Gomez et al. 2007). Figure reproduced from Guimard et. al. with permission of Elsevier.

Electrochemical synthesis of conducting polymers is common as it is relatively straightforward and can produce thin films with controlled thickness. This process uses a three-electrode set up (working, counter, and reference electrodes) in a solution containing the monomer, dopant, and solvent. Current or voltage is passed through the solution, and electrodeposition occurs at the working electrode as monomer is oxidized to form radical cations that react with other monomers or radical cations and form an insoluble polymer (**Figure 3**) (Guimard, Gomez et al. 2007). The deposition time, temperature, solvent, dopant, and electrode materials are common factors that can be adjusted to affect the resulting polymer.

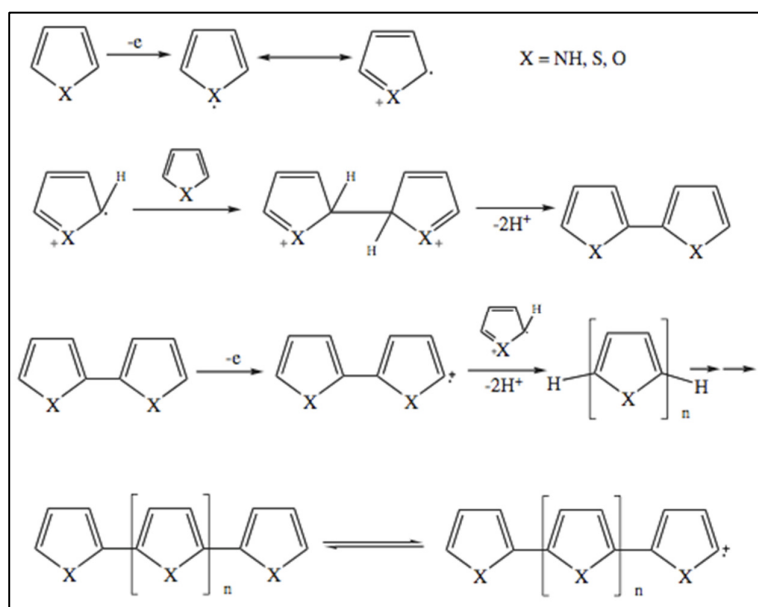


**Figure 3.** Mechanism of electrochemical polymerization initiated by oxidation of monomer at working electrode (Guimard, Gomez et al. 2007). Figure reproduced from Guimard et. al. with permission of Elsevier.

Polypyrrole (PPy) and poly(3,4-ethylene dioxythiophene) (PEDOT) are two commonly studied conducting polymers in battery technology, photovoltaic devices, light emitting diodes (Gurunathan, Murugan et al. 1999), and biomedical applications such as drug delivery (Abidian, Kim et al. 2006), biosensors (Wallace, Smyth et al. 1999; Gerard, Chaubey et al. 2002), neural recording (Ludwig, Uram et al. 2006), tissue engineering (Gomez, Lee et al. 2007; Lundin, Herland et al. 2011), and bio-actuators (Smela 2008). Conducting polymers are attractive alternatives to conventional electronic materials for neural interfaces due to their ability to be functionalized with biomolecules (Ahuja, Mir et al. 2007), their ionic and electronic conductivity (Cogan 2008), their relatively soft mechanical properties (Green, Lovell et al. 2008) and the ease of altering their electrical, chemical, and physical properties (Guimard, Gomez et al. 2007). PPy and PEDOT have exhibited good biocompatibility. While PPy has commonly been used in neural interface applications due to the solubility of the pyrrole monomer in water, PEDOT exhibits very high conductivity and chemical stability (Fattahi, Yang et al. 2014).

The feasibility of using conducting polymers as substrates for neural cell attachment and proliferation may depend on the dopant used and the electrical charge of the conducting polymer. It has been shown that neural stem cell proliferation and differentiation on PPy substrates with dodecylbenzenesulfonate (DBS) as the dopant were comparable to those cells on standard tissue culture polystyrene. However, reduction of the PPy films decreased the

neural stem cell viability and led to cell death. This reaction is thought to be due to changes in conformation of adsorbed proteins such as fibronectin on the PPy films (Lundin, Herland et al. 2011).

Various drugs and biomolecules have been incorporated into conducting polymers to increase biocompatibility and/or reduce fibrotic encapsulation. Such biomolecules can be incorporated either as charged dopants or as non-dopant inclusions during the polymerization process. Biological dopants have included laminin peptides, hyaluronic acid, and fibronectin fragments, and polysaccharides, while non-dopant inclusions have included neurotrophins, human serum albumin, and whole laminin (Green, Lovell et al. 2008).

Conducting polymers can provide actively controlled release of such molecules as well. As conducting polymers undergo redox reactions, the charging and discharging of the polymer is accompanied by the movement of solvent and/or ions into or out of the polymer (Smela 2003). This unique feature allows conducting polymers to release biomolecules that have been incorporated into their structure. For example, dexamethasone, an anti-inflammatory drug, has been incorporated into the lumen of conducting polymer nanotubes. Electrical actuation of the conducting polymer results in expansion and contraction of the cavity thereby controllably releasing the dexamethasone (Abidian, Kim et al. 2006).

In addition, conducting polymers can improve the electrical properties of neural interface materials used for neural stimulation and recording. There is an inherent trade-off between the size of the electrode (selectivity) and the electrical properties (sensitivity); while smaller electrodes are more spatially selective, they suffer from increased impedance and decreased injection charge density (Cogan 2008). The application of conducting polymer to the surface of a traditional metal electrode increases the effective surface area available for ionic-to-electronic charge transfer thereby reducing impedance and increasing injection charge density (Abidian, Corey et al. 2010).

This effect can be further enhanced by the use of conducting polymer nanostructures. Conducting polymer nanofibers and nanotubes have been fabricated using a templating technique, and PEDOT nanotube-coated electrode sites reduced the impedance approximately two orders of magnitude lower than uncoated gold electrode sites (at 1 kHz). Additionally, the charge injection density increased from  $0.001 \pm 10^{-4} \mu\text{C}$  for bare gold electrodes to  $4.9 \pm 0.6 \mu\text{C}$  for PEDOT nanotube-coated electrodes (Abidian, Corey et al. 2010). Such conducting polymer nanotubes have been used for actuated drug delivery (Abidian, Kim et al. 2006), neural recording (Abidian, Ludwig et al. 2009), and substrates for neurite growth (Abidian, Corey et al. 2010).

### 1.3 Electrospinning in Biomedical Applications

Electrospinning is a method for fabricating nanofibers, similar to the commercial process of drawing microscale fibers except that it uses electrostatic repulsions between surface charges rather than a mechanical force to continuously reduce the diameter of a viscoelastic jet (Li and Xia 2004). Electrospinning uses a high voltage to induce the formation of an electrified polymer jet from the polymer solution as the solvent rapidly evaporates. A solid fiber is generated as the polymer jet is stretched due to electrostatic repulsions, in turn leaving a polymer fiber mat (**Figure 4**).

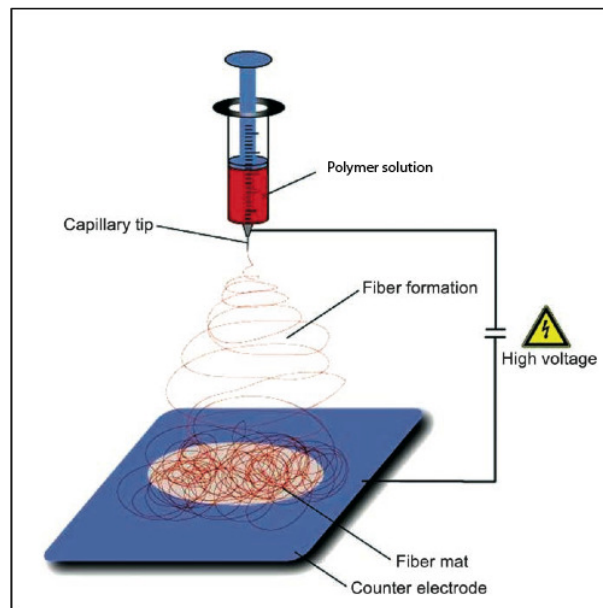


**Figure 4.** Electrospinning is a fabrication method that uses high voltages to spray a polymer solution onto a stationary target where it is collected as a random fiber mat or onto a rotating wheel where it is collected as aligned fibers (Greiner and Wendorff 2007). Figure reproduced from Greiner et. al. with permission of John Wiley & Sons.

The electrospinning set up requires a high voltage power supply, a metallic capillary tip through which the polymer solution is pumped, and a grounded collector (counter electrode). Polymer solution is fed through the metallic tip at a controlled rate, and the high voltage applied to the tip causes charge built up on the polymer solution droplet. The droplet is subject both to electrostatic repulsion between the surface charges on the drop and to a Coulombic force exerted by the applied electric field. Once the applied electric field is strong enough, the electrostatic forces cause the polymer drop to form an electrified polymer jet leading to a long and thin fiber. This fiber is attracted to the grounded collector where it forms a polymer fiber mat (Li and Xia 2004).

The electrospinning process allows control over fiber diameter, composition, and spatial alignment (Li and Xia 2004). Fiber diameter is typically determined by the type of polymer, the solution viscosity and electrical conductivity, and the operational conditions such as electric field, polymer feed rate, and temperature (Li and Xia 2004). For example, if the polymer viscosity is not great enough, beading and droplets are observed rather than uniform fibers, while if the polymer viscosity is too high, the polymer drop will dry out before it forms a jet, thereby preventing electrospinning. Polymer solutions with lower viscosity tend to produce fibers with smaller diameters. Likewise, lower flow rates and higher temperatures tend to yield fibers with smaller diameters (Li and Xia 2004; Pham, Sharma et al. 2006).

Composition of electrospun fibers has included ceramics oxides such as  $\text{SiO}_2$  and  $\text{Al}_2\text{O}_3$ , functional polymers such as conductive polyaniline and piezoelectric poly(vinylidene fluoride), biodegradable polymers such as poly(caprolactone) and poly(L-lactide), and natural biopolymers such as DNA, silk, and collagen. Composition can further be modified by encapsulation of functional materials within the nanofibers such as inclusion of carbon nanotubes (CNTs) in electrospun nanofibers to increase mechanical strength and electrical conductivity (Li and Xia 2004).

Secondary structure and spatial alignment of electrospun fibers can be adjusted by using different processing conditions and set ups. For example, core/sheath structures have been created by using a mixture of two polymers that will separate as the solvent is evaporated during electrospinning or by using a coaxial metallic tip. Additionally, aligned nanofibers have been created by replacing the grounded collector with a rotating drum or a pair of split electrodes (Li and Xia 2004).

Electrospun nanofibers have found applications in biomedical engineering for wound dressing, drug delivery, and specifically tissue engineering (Li and Xia 2004). Tissue engineering attempts to mimic the mechanical and biological properties of the native extracellular matrix, which is mostly composed of a network of nanometer-sized proteins and glycosaminoglycans (Pham, Sharma et al. 2006). This environment provides important cell signaling cues and modulates cellular activities such as migration, proliferation, differentiation, and gene expression. A variety of biopolymers and biodegradable polymers have been electrospun for use as tissue engineering scaffolds (Pham, Sharma et al. 2006).

Within the field of neural interfacing, electrospun nanofibers in the 400-600 nm diameter range have been shown to orient dorsal root ganglia and Schwann cells *in vitro*. Additionally, the size of the electrospun fibers affected the cellular response; while both

micro- and nanoscale fibers could orient neural stem cells, the nanoscale fibers increased the stem cell differentiation and increased the neurite length (Hoffman-Kim, Mitchel et al. 2010).

## 1.4 Conducting Polymer – Hydrogel Blends

While conducting polymers have shown much promise in neural interface applications, the development of conducting polymer-hydrogel blends has been proposed to improve mechanical properties and provide a reservoir for water soluble biomolecules (Green, Baek et al. 2010). Due to their high water content, hydrogels often closely match the mechanical properties of soft biological tissues. Additionally, they tend to resist protein deposition, which could modulate the fibrotic response associated with implanted materials (Green, Baek et al. 2010).

Conducting polymer-hydrogel blends can be fabricated by forming a hydrogel matrix and then electrochemically depositing conducting polymer within the hydrogel (Green, Baek et al. 2010; Sekine, Ido et al. 2010; Abidian, Daneshvar et al. 2012). This unique structure can be accomplished by placing the hydrogel on a working electrode and providing conducting polymer monomer and dopants within the hydrogel (**Figure 5**). Using this method, conducting polymer can be grown uniformly from the working electrode and then separated from the electrode by actuation (Sekine, Ido et al. 2010).

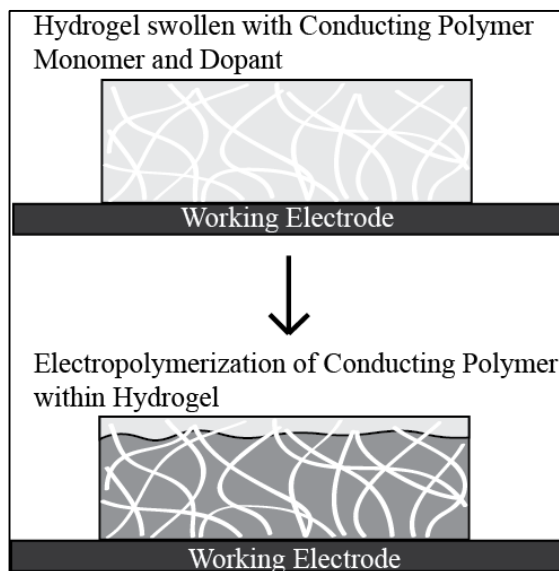


**Figure 5.** Fabrication of conducting polymer – hydrogel blend by electropolymerization of conducting polymer within a polymerized hydrogel.

Conducting polymer-hydrogel blends have been shown to be effective in cell stimulation. Electrodes of PEDOT printed on an agarose gel sheet were found to have a surface resistance of  $11 \text{ k}\Omega/\square$  and could be stored in water for over one month. These electrodes were used to stimulate C2C12 myotubes resulting in cellular contraction (Sekine, Ido et al. 2010). Similar materials have also been beneficial in nerve regeneration applications. Polypyrrole-oligo(polyethylene glycol) fumarate scaffolds were shown to support cell attachment and neurite growth (Runge, Dadsetan et al. 2010), and the use of PEDOT-agarose conduits in a rat peroneal nerve gap model resulted in robust axonal regeneration with mature, large diameter, myelinated axons (Abidian, Daneshvar et al. 2012).

## **Chapter 2. CONDUCTING POLYMER NANOFIBERS FOR SENSITIVE DETECTION OF GLUCOSE**

Sensitive detection and selective determination of the physiologically important chemicals involved in brain function have drawn much attention for the diagnosis and treatment of brain diseases and neurological disorders (Adams 1976; Burdette and Lippard 2003; Wei, Bailey et al. 2009). In particular, monitoring changes in extracellular glucose concentration that is indicative of glucose metabolism in the brain may improve diagnosis of and therapy for brain tumors (Li 1982; Wang, Volkow et al. 1996; Namba, Iwadata et al. 1998) and assist in understanding physiological changes following traumatic brain injuries (De Fazio, Rammo et al. 2011). In addition to the significance of glucose monitoring in brain disease and neurological disorders, it is the key analyte for medical diagnosis and management of diabetes, which affects nearly 26 million Americans (Prevention 2011).

To date, the most common glucose biosensors achieve specific recognition of glucose by immobilization of the enzyme glucose oxidase (GOx) on the surface of electrodes. Although a number of methods have been developed for immobilization of GOx (Arica and Hasirci 1993; Foulds and Lowe 1986; Gursel and Hasirci 1992; Hinberg, Kapoulas et al. 1974) and detection of glucose (Bindra and Wilson 1989; Park, Chung et al. 2003; Wingard, Castner et al. 1984) achieving high sensitivity and longevity in these biosensors has remained a challenge.

In biosensors using an enzyme as the biorecognition element, the issues of sensitivity and longevity are functions of the physical design and of enzyme stability over time (Wilson and Gifford 2005). As electrodes become smaller, into the micro- and nano- scale, they provide better spatial resolution for recording chemical signals in the brain compared to larger electrodes, have faster electron kinetics (Balasubramanian 2010) with small RC time constants that enable high temporal resolution, and have reduced background noise leading to higher signal-to-noise ratios (Wei, Bailey et al. 2009). However, they also suffer from the problem of high impedance due to their small feature geometry (Robinson 1968). The challenge in developing chronic glucose biosensors arises from the inherent instability of GOx and the leaching of the enzyme from the electrode surface. Adding to the challenge, GOx can be inactivated by hydrogen peroxide that is produced during the oxidation of glucose to gluconic acid (Fortier and Belanger 1991).

The application of conducting polymer to electrode surfaces has gained considerable attention as a means to address these challenges by increasing the signal-to-noise ratio,

servicing as a suitable matrix for the immobilization and entrapment of enzymes, and facilitating direct electron transfer during chemical detection (Sangodkar, Sukeerthi et al. 1996; Gerard, Chaubey et al. 2002; Ramanavicius, Ramanaviciene et al. 2006). Among different conducting polymers, poly(3,4-ethylenedioxythiophene) PEDOT has been reported to exhibit superior chemical stability and high conductivity (Yamato, Ohwa et al. 1995; Groenendaal, Jonas et al. 2000; Groenendaal, Zotti et al. 2003; Kros, Sommerdijk et al. 2005), which has led to its successful use in amperometric biosensors (Kros, Nolte et al. 2002).

In addition to the use of new electrode materials, the ability to fabricate nanostructures at the recording site allows for new physical designs of the biosensor. Nanostructured sensing elements provide higher sensitivity as a result of increased surface to volume ratio (Balasubramanian 2010), and PEDOT nanostructures have provided a decrease in impedance at recording sites by 77% compared to PEDOT film (Abidian, Corey et al. 2010). Finally, PEDOT nanostructures have been shown to increase the percentage of sites having high-quality recordings during chronic neural recording (Abidian, Ludwig et al. 2009) making them good candidates for use in chronic glucose biosensors.

In the present work, GOx entrapped in PEDOT was prepared in films as well as in nanofibers and the electrical properties, sensitivity, and longevity of each type of sensor was measured at polarization potentials of +300mV and +700mV vs. Ag/AgCl. Each structure directly entrapped GOx in PEDOT during galvanostatic polymerization at the electrode site. Galvanostatic polymerization of the PEDOT was used to control the rate of polymerization, while a supporting electrolyte was included to facilitate GOx incorporation into the polymer. (Wallace, Smyth et al. 1999) During polymerization, GOx becomes immobilized in the porous PEDOT by a combination of physical entrapment and polymer charge balance, with the enzyme acting as a counterion (electrostatic interactions) (Ahuja, Mir et al. 2007). Entrapment during electropolymerization is a reproducible method that allows for spatially controlled deposition (Ahuja, Mir et al. 2007) and may improve the enzyme's activity and stability compared to a covalent binding method. Enzyme entrapment also eliminates the use of harsh chemicals typically used to covalently bind enzymes to the surface of electrodes. Other studies have shown that GOx retains its functionality after entrapment in conducting polymer, follows typical Michaelis-Menten kinetics, and is actually more resistant to denaturation from changes in pH or temperature than soluble GOx (Hinberg, Kapoulas et al. 1974).

## 2.1 Materials & Methods

A solution containing 0.02M 3,4-ethylene dioxythiophene (EDOT) monomer, 0.6mM poly(sodium-p-styrene sulfonate), 1mM poly(ethylene glycol) (M.W. 3000), and 1,000U/ml glucose oxidase Type VII was prepared in DI water. The PEDOT film + GOx sensors were fabricated by electrochemical polymerization in the above solution carried out at galvanostatically at 0.5mA/cm<sup>2</sup> for 300s directly on microelectrode arrays using an Ag/AgCl reference electrode and Pt counter electrode.

To fabricate the PEDOT nanofibers + GOx, poly(L-lactide) (PLLA) nanofibers were first directly electrspun on microelectrode arrays from a solution of 7.8% (w/v) poly(L-lactide) (PLLA) with an inherent viscosity of 3.3-4.3 dLg<sup>-1</sup> in chloroform. The solution was stirred at a temperature of 50°C for 10hr prior to electrospinning in order to produce a homogenous solution. The electrospinning process was carried out in an electrical field of 0.6kV/cm with a flow rate of 0.25mL/hr for 30s, and the electrodes were held at a distance of 15cm from the syringe needle during this process. This electrospinning was followed by the electrochemical deposition of PEDOT+ GOx in the same manner as the films.

Fourier transform infrared spectroscopy (FTIR) spectra were used to characterize whether the major component of the nanofibers is affected by the incorporation of GOx. They were recorded on a computer controlled Bruker Vertex70 FTIR spectrometer with “MVP-Pro” Attenuated Total Reflectance accessories (resolution=4 cm<sup>-1</sup>, scan time=100). The wavenumber range was 400-4000 cm<sup>-1</sup>.

Electrochemical quartz crystal microbalance (EQCM) experiments to determine the quantity of GOx enzyme in PEDOT film and PEDOT nanofiber were done on a 0.33 cm<sup>2</sup> EQCM crystal (6MHz, Pt/TiO<sub>2</sub>, polished, Metrohm, USA) using Autolab PGSTAT 302N at 20 °C. The frequency change can be related to the mass change by the Sauerbrey equation:

$$\Delta f = -C_f \cdot \Delta m$$

where  $\Delta f$  is the frequency change (Hz),  $C_f$  is the sensitivity factor (0.0815 Hz·ng<sup>-1</sup>·cm<sup>2</sup> for this 6 MHz crystal at 20 °C), and  $\Delta m$  is the mass change (ng). The mass of entrapped enzyme was calculated by comparison between the mass of unmodified PEDOT (without GOx) and modified PEDOT (GOx incorporated) assuming that a constant electrodeposition charge does not impede the electrodeposition (Piro, Dang et al. 2001).

Impedance spectroscopy was performed using an Autolab PGSTAT-12. Impedance spectra of bare platinum electrode sites as well as sites with PEDOT film + GOx and PEDOT nanofiber + GOx were recorded. A solution of phosphate buffered solution (PBS, 0.1M,

pH=7) was used as an electrolyte in a three-electrode cell configuration. The counter electrode was platinum foil and an Ag/AgCl reference electrode was used. An AC sinusoidal signal with 5mV amplitude was used to record impedance of a frequency range of 1-10<sup>5</sup> Hz.

An eDAQ Quadstat was used to record the amperometric response of bare platinum electrode sites, PEDOT film + GOx sensors, and PEDOT nanofiber + GOx sensors to injections of glucose. A stirred solution of PBS (0.1M, pH = 7) was used as an electrolyte in a three-electrode cell configuration. The counter electrode was platinum foil and an Ag/AgCl reference electrode was used. A polarization potential of either +300mV or +700mV was applied to the working electrode. Once the background current stabilized, increasing amounts of glucose solution was injected to the stirred PBS solution. The resulting current measurements were used to calculate the sensitivity, limit of detection, and response time.

Finally, cyclic voltammetry (CV) was measured using an Autolab PGSTAT 12 instrument. The potential applied to the working electrode was swept from -1 to 1.6 V with scanning rate of 100 mV s<sup>-1</sup>, and the charge storage capacity (CSC) was calculated using Origin software. The CV test was performed immediately after the applied constant potential for the electroactivity loss study. The electroactivity change over 280 minutes was measured, which corresponds to the total time the sensors were potentiostated for sensitivity measurements over 30 days.

## 2.2 Results & Discussion

The PEDOT films + GOx sensors were the result of electrodeposition from a solution containing EDOT monomer, poly(sodium-p-styrene sulfonate), and glucose oxidase directly on microelectrode arrays (**Figure 6**). The PEDOT nanofibers + GOx were fabricated by first electrospinning poly(L-lactide) (PLLA) nanofibers directly on microelectrode arrays. This electrospinning was followed by the electrochemical deposition of PEDOT + GOx in the same manner as the films (**Figure 7 & 8**).

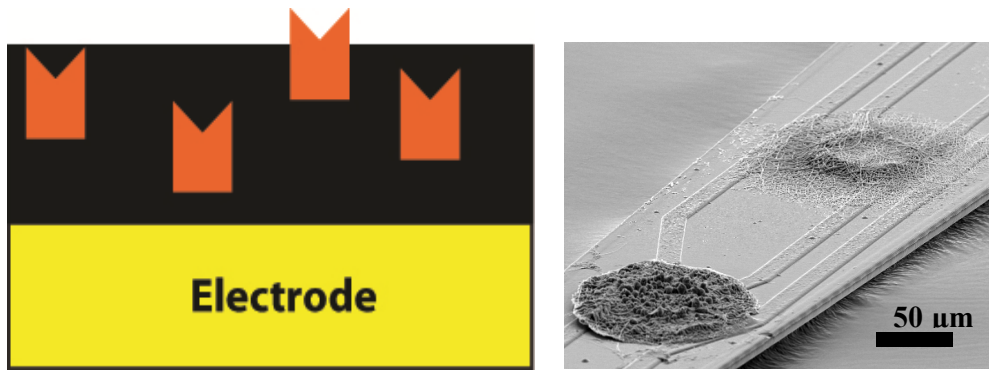


**Figure 6.** Schematic illustration PEDOT film + GOx coated microelectrodes. SEM image of PEDOT film and PEDOT nanofibers on neural electrode.

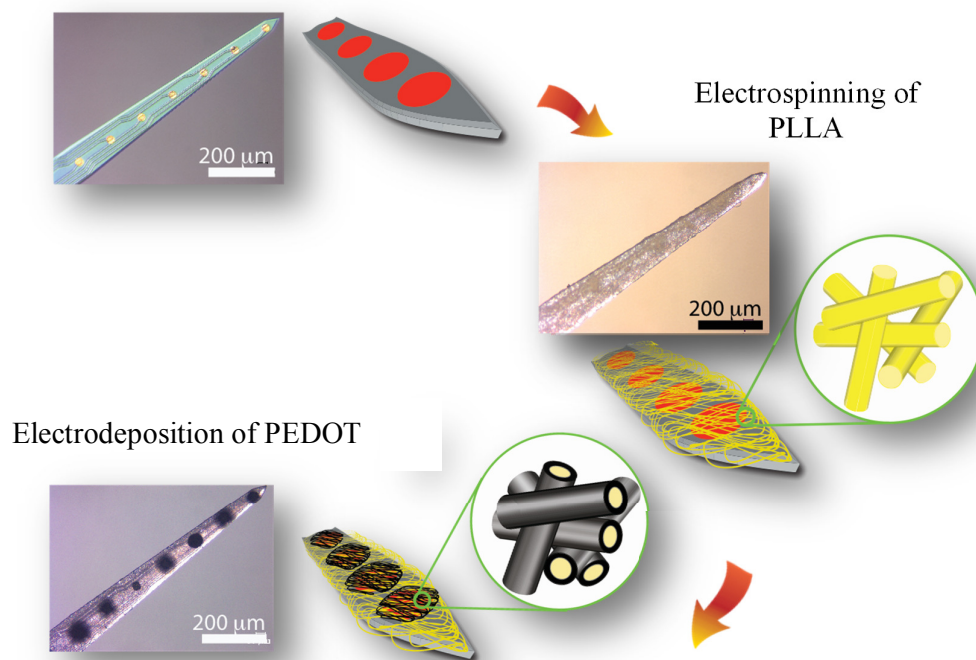


**Figure 7.** Schematic illustration of fabrication process of PEDOT nanofibers showing electrospinning of PLLA template fibers followed by electrodeposition of PEDOT around the fibers at electrode site (Abidian, Kim et al. 2006). Optical images are representative of the fabrication process. Figure adapted from Abidian et. al. with permission of John Wiley & Sons.

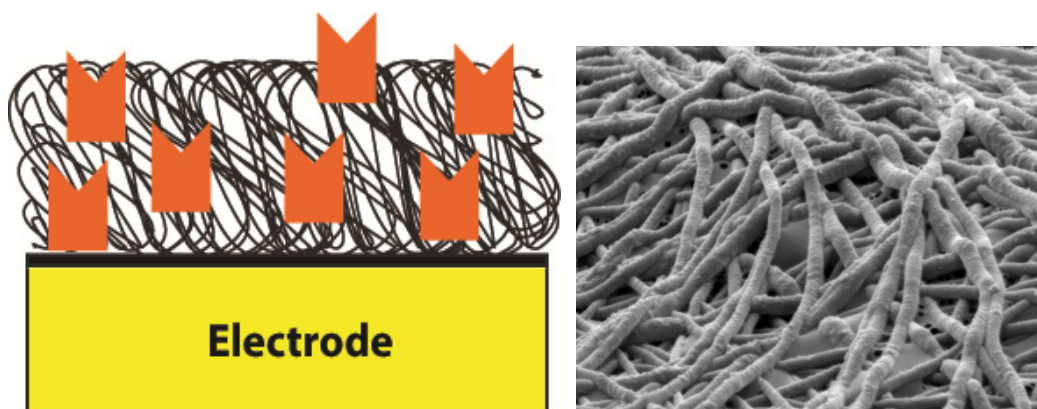


**Figure 8.** Schematic illustration image of PEDOT nanofiber + GOx. SEM image representative of PEDOT nanofibers.

Scanning electron microscope (SEM) images were used to measure the thickness of the resulting PEDOT film + GOx sensors and the diameter of the fibers on the PEDOT nanofiber + GOx sensors. The films had a thickness of  $100 \pm 5$  nm and the PEDOT coated nanofibers had an outer diameter of  $110 \pm 8$  nm with a core diameter of  $80 \pm 8$  nm, which represents the diameter of electrospun PLLA nanofibers.

To characterize whether the major component of the nanofibers is affected by the incorporation of GOx, fourier transform infrared spectroscopy (FTIR) was performed on PEDOT nanofibers with and without GOx (**Figure 9**). The resulting spectra showed absorption bands at  $1162\text{ cm}^{-1}$ ,  $1121\text{ cm}^{-1}$  and  $1066\text{ cm}^{-1}$ , which are assigned to the stretching vibration of the ethylenedioxy group. The C-S vibration absorption can be seen at  $947\text{ cm}^{-1}$ ,  $860\text{ cm}^{-1}$  and  $712\text{ cm}^{-1}$ . The C-C and C=C absorption in the thiophene ring is at  $1345\text{ cm}^{-1}$  and  $1501\text{ cm}^{-1}$ . There is no significant difference between PEDOT nanofibers without GOx and PEDOT nanofibers + GOx, showing that the major component of the polymer matrix is PEDOT and that incorporation of GOx does not interfere with the electropolymerization process (Piro, Dang et al. 2001).

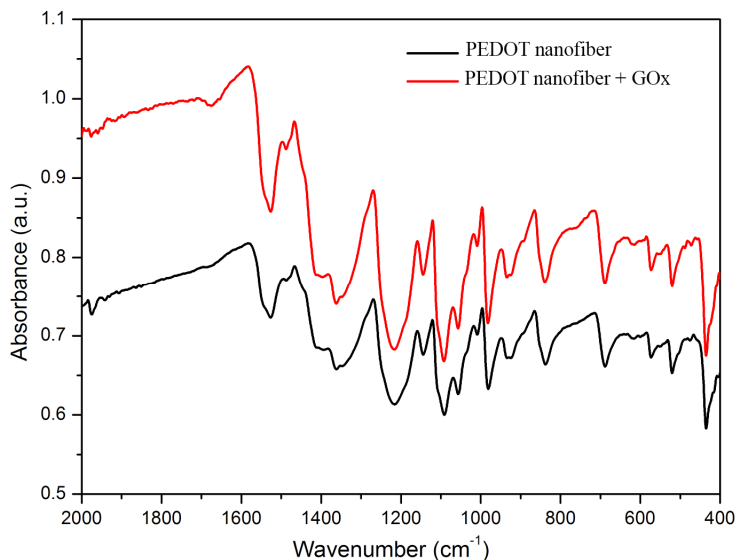


**Figure 9.** FTIR spectrum of PEDOT nanofibers with and without GOx.

To determine the quantity of GOx enzyme in PEDOT film and PEDOT nanofiber, electrochemical quartz microbalance (EQCM) experiments were performed. EQCM results revealed that the amount of GOx incorporated in PEDOT nanofibers was  $31\mu\text{g cm}^{-2}$ , significantly more than the  $1.3\mu\text{g cm}^{-2}$  of GOx incorporated in PEDOT film (**Figure 10**). The increase in amount of GOx in the PEDOT nanofibers compared to the PEDOT films could be due to a combination of two factors: first, an increase in the effective surface area available to entrap GOx on the PEDOT nanofibers, and second, an electrostatic interaction between the positively charged PLLA nanofibers and the negatively charged GOx (Shaolin, Huaiguo et al. 1991). EQCM has been employed by others to measure entrapped GOx in PEDOT during electropolymerization, and in agreement with the abovementioned FTIR measurements, these results demonstrated that GOx did not affect the electropolymerization of the PEDOT (Piro, Dang et al. 2001).

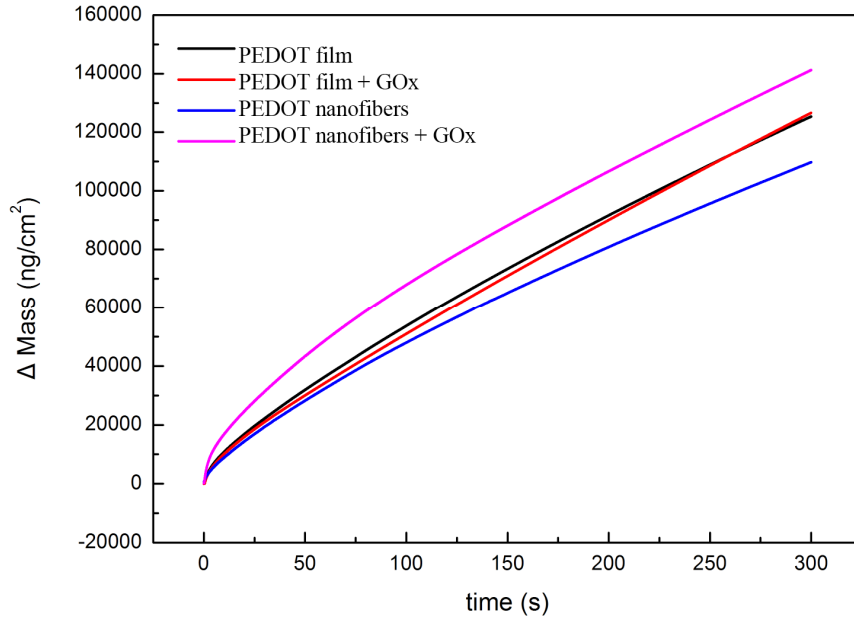


**Figure 10.** EQCM showing significantly more GOx incorporated into PEDOT nanofiber + GOx sensors compared to PEDOT film + GOx sensors.

Once the fabrication of the glucose sensors was characterized, the impedance of these sensors was measured. It has been shown that conducting polymer films can significantly decrease the impedance of neural recording sites of implanted microelectrodes and that PEDOT nanostructures further reduce impedance at such sites compared to PEDOT films (Abidian, Corey et al. 2010). The reduction in impedance by PEDOT nanofibers compared to PEDOT films is due to the relative increase in electrode surface area provided by the nanofibers. In order to confirm that the inclusion of GOx in the biosensors would not affect this phenomenon, the impedance spectra of bare platinum electrode sites was compared to the impedance spectra of PEDOT film + GOx and PEDOT nanofiber + GOx sensors (**Figure 11**).

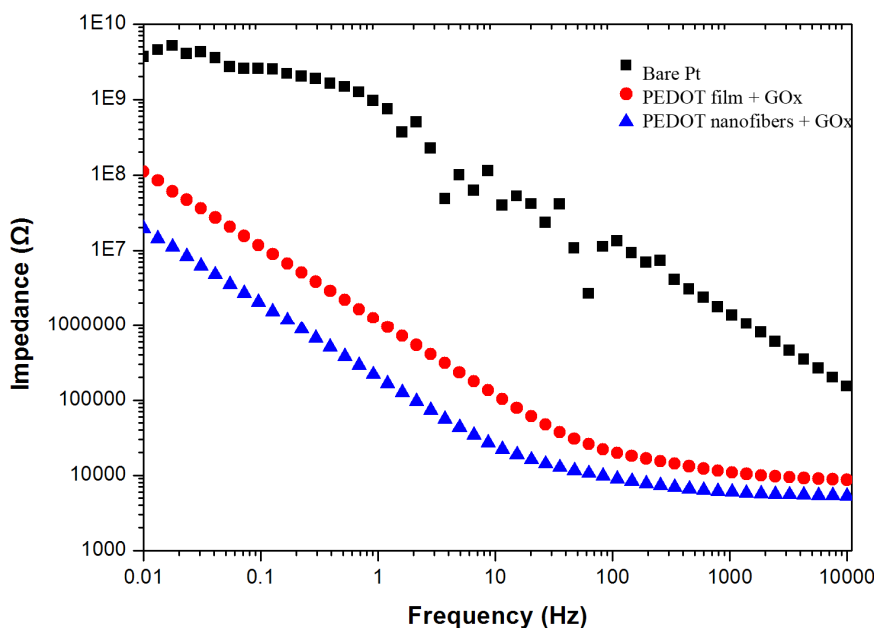


**Figure 11.** Impedance spectrum of bare platinum electrode sites compared to sites with PEDOT + GOx film and PEDOT + GOx nanofibers.

Over all frequencies measured, the PEDOT nanofibers + GOx had lower impedance than the PEDOT film + GOx. Since the sensitivity of the PEDOT film + GOx and PEDOT nanofiber + GOx sensors as described later was measured with a constant polarization potential, the impedance at low frequency (0.01 Hz) was estimated. At this low frequency, the impedance of the PEDOT film + GOx sensors was approximately 100 M $\Omega$  and that of the PEDOT nanofiber + GOx sensors was approximately 12.5 M $\Omega$ , representing a 87.5% reduction in impedance by the nanofiber morphology compared to the film morphology. For comparison, the impedance at 0.01 Hz for a bare platinum electrode was approximately 1,995 M $\Omega$ . These impedance changes are very comparable to those changes seen when electrode sites were modified with PEDOT film and PEDOT nanostructures without GOx (Abidian, Corey et al. 2010).

The reduction in impedance from PEDOT film + GOx compared to PEDOT nanofiber + GOx sensors in combination with the increased entrapment of GOx in the PEDOT nanofibers was expected to directly increase the sensitivity of the nanostructured sensors. To measure sensitivity, polarization potentials of +300 mV or +700 mV vs. Ag/AgCl were applied to the each type of sensor in a stirred solution of PBS while injections of increasing amounts of glucose were made. The resulting change in current was measured. At polarization potentials of either +300 mV or +700 mV, the PEDOT nanofiber + GOx sensors showed a larger

amperometric response to the glucose injections than the PEDOT film + GOx sensors (Figure 12).

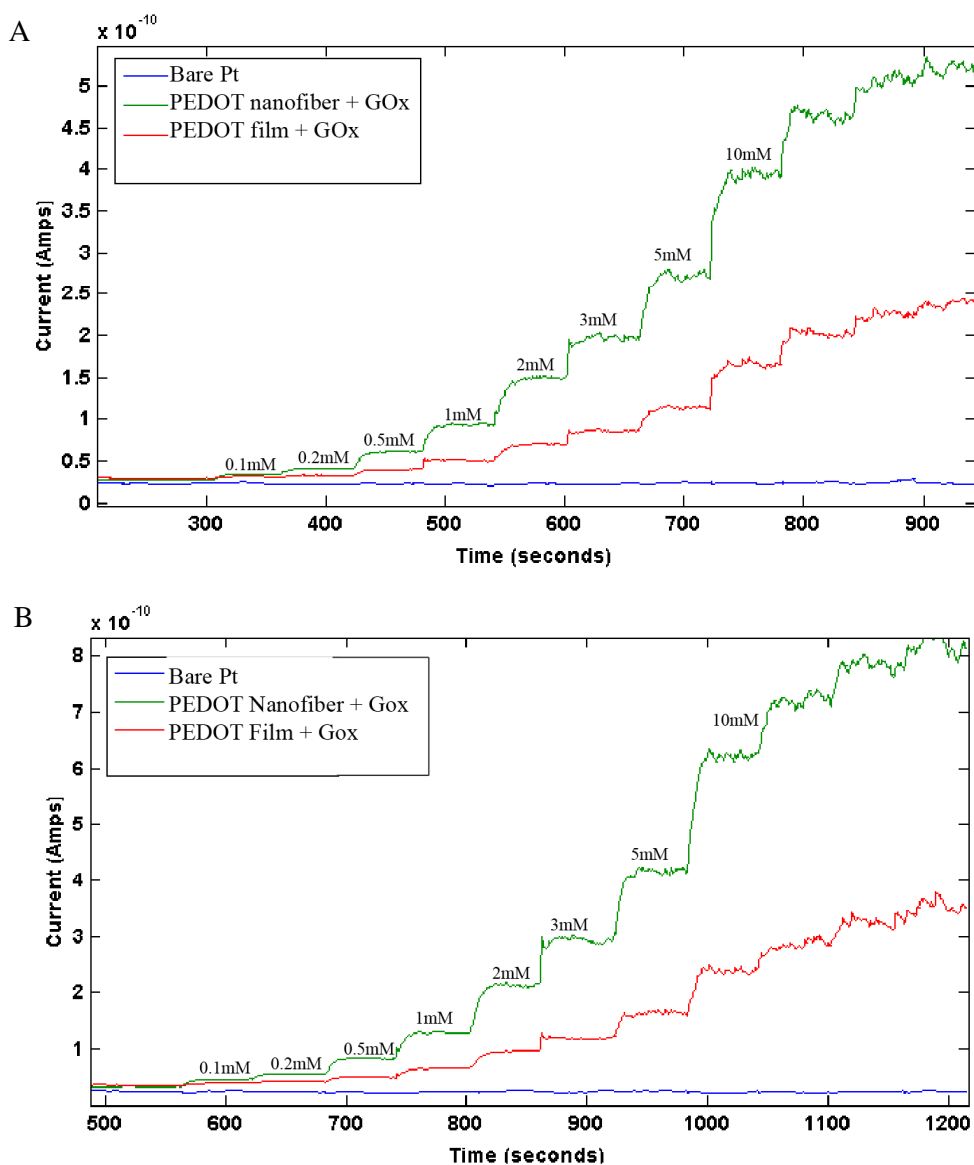


**Figure 12.** Amperometric response of PEDOT film + GOx and PEDOT nanofiber + GOx to serial injections of glucose at + 300 mV (A) and + 700 mV (B).

To quantify the amperometric response, calibration curves for each sensor were created (Figure 13) relating the current to the glucose concentration. While glucose concentrations ranging from 0.1 mM to 25mM were tested, the sensors were found to have a linear range of up to 5 mM glucose. Other glucose sensors based on entrapping GOx within conducting polymer have achieved linear ranges of up to 10 – 25 mM (Belanger, Nadreau et al. 1989; Piro, Dang et al. 2001; Nien, Tung et al. 2006); however, based on the biological range of

glucose concentrations, a sensor with a linear range of up to 5 mM is suitable for measuring glucose in cerebrospinal fluid where glucose concentrations are typically 2/3 that of their concentration in blood plasma (Medicine 2014).

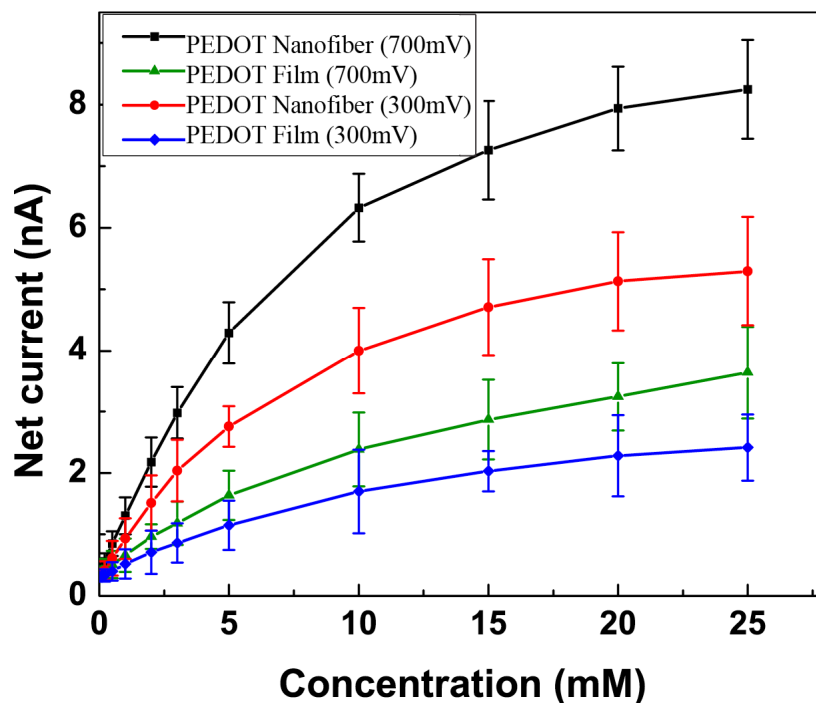


**Figure 13.** Amperometric response curves of PEDOT + GOx films and PEDOT + GOx nanofiber sensors at +300mV and +700mV polarization potentials.

Using the linear response range, the sensitivity was calculated for each type of sensor at each polarization potential as the amperometric response per mM of glucose per  $\text{cm}^2$  area of the sensor. At +300 mV, the initial sensitivity of PEDOT film + GOx was  $1.2 \pm 0.5 \mu\text{A cm}^{-2} \text{mM}^{-1}$ , while that of the PEDOT nanofiber + GOx was  $6.4 \pm 0.8 \mu\text{A cm}^{-2} \text{mM}^{-1}$ , representing a 433% increase in sensitivity. Similarly, at +700mV, the initial sensitivity of PEDOT film + GOx was  $3.6 \pm 0.8 \mu\text{A cm}^{-2} \text{mM}^{-1}$ , while that of the PEDOT nanofiber + GOx was  $9.2 \pm 1.1 \mu\text{A cm}^{-2} \text{mM}^{-1}$ , representing a 156% increase in sensitivity (**Figure 14**). At both polarization potentials, the change in sensitivity from the PEDOT film + GOx samples compared to the PEDOT nanofiber + GOx samples was statistically significant ( $p < 0.0001$ ). The increased surface area associated with using PEDOT nanofiber + GOx rather than PEDOT film + GOx has a dual effect; first, it decreases the impedance of the sensor, and second, it allows more GOx to be entrapped on the sensor; both of these results contribute to the increased

sensitivity of the PEDOT nanofibers + GOx sensors compared to the PEDOT film + GOx sensors.

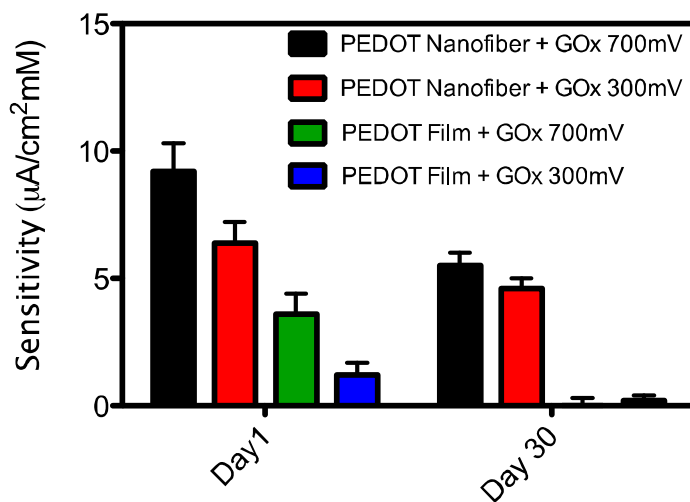


**Figure 14.** Sensitivity of PEDOT film + GOx sensors and PEDOT nanofiber + GOx sensors at + 300mV and + 700mV polarization potentials at Day 1 and Day 30.

In addition to improved sensitivity, the PEDOT nanofiber + GOx sensors also showed a lower limit of detection of glucose than the PEDOT film + GOx sensors. At +300 mV, the limit of detection of PEDOT film + GOx was 0.56 mM glucose, while that of the PEDOT nanofiber + GOx was 0.26 mM glucose. Increasing the potential to + 700 mV, resulted in the limit of detection of the PEDOT film + GOx to decrease to 0.45 mM glucose and that of the PEDOT nanofiber + GOx to decrease to 0.12 mM glucose. All of these limits of detection fall below the biological range of glucose concentrations, both in cerebrospinal fluid and in blood plasma.

The +700 mV polarization potential resulted in statistically significant higher sensitivities and lower limits of detection than the +300 mV polarization potential for both the PEDOT film + GOx and the PEDOT nanofiber + GOx sensors ( $p < 0.0001$ ). However, the improvement in sensitivity for the nanofiber sensors compared to the film sensors at each potential was not equivalent (433% increase compared to a 156% increase for +300mV and +700mV respectively). It is possible that when using + 700 mV, the benefits of the nanostructured sensor are mitigated by the increased reoxidation of hydrogen peroxide, a by-product of glucose oxidation, at higher polarization potentials resulting in a loss of activity of GOx (Fortier and Belanger 1991). For example, at +300mV and +700mV, a bare platinum electrode in GOx and 10mM glucose solution measured a current of 0.0564 nA and 0.5602

nA respectively. It has been shown that hydrogen peroxide can be oxidized at a platinum electrode with potentials as low as +200 mV (Belanger, Nadreau et al. 1989).

While using lower polarization potentials results in less sensitivity at the start of recording, it could still be desirable if it could increase the lifetime of the sensor. The use of a lower polarization potential of +300 mV was based on the expectation that a lower polarization potential could possibly increase the lifetime of the sensor by either preserving the activity of the GOx through less oxidation of hydrogen peroxide or by extending the electroactivity of the conducting polymer. It has been demonstrated that glucose can be detected at a potential of +350 mV (Ag/AgCl reference) in a sensor that was highly selective with respect to other substrates and with a response independent of oxygen concentration (Koopal, Feiters et al. 1992).

The longevity of the electrodes was measured as the electrodes' sensitivities over the course of 30 days (**Figure 15**). Electrodes were stored at 4 °C in PBS between measurements. At +700 mV, the PEDOT film + GOx and PEDOT nanofiber + GOx biosensors showed a decrease in sensitivity of 99% (from  $3.6 \pm 0.8 \mu\text{A cm}^{-2} \text{mM}^{-1}$  to  $0.01 \pm 0.3 \mu\text{A cm}^{-2} \text{mM}^{-1}$ ) and 40% (from  $9.2 \pm 1.1 \mu\text{A cm}^{-2} \text{mM}^{-1}$  to  $5.5 \pm 0.5 \mu\text{A cm}^{-2} \text{mM}^{-1}$ ) respectively over the 30 days. Reducing the polarization potential to +300 mV improved the longevity of the sensors and resulted in a drop in sensitivity of 83% (from  $1.2 \pm 0.5 \mu\text{A cm}^{-2} \text{mM}^{-1}$  to  $0.2 \pm 0.2 \mu\text{A cm}^{-2} \text{mM}^{-1}$ ) for the PEDOT film + GOx and 28% (from  $6.4 \pm 0.8 \mu\text{A cm}^{-2} \text{mM}^{-1}$  to  $4.6 \pm 0.4 \mu\text{A cm}^{-2} \text{mM}^{-1}$ ) for the PEDOT nanofiber + GOx sensors. Interestingly, the PEDOT nanofiber + GOx sensors experienced a smaller loss in sensitivity at both potentials than the PEDOT film + GOx sensors did.

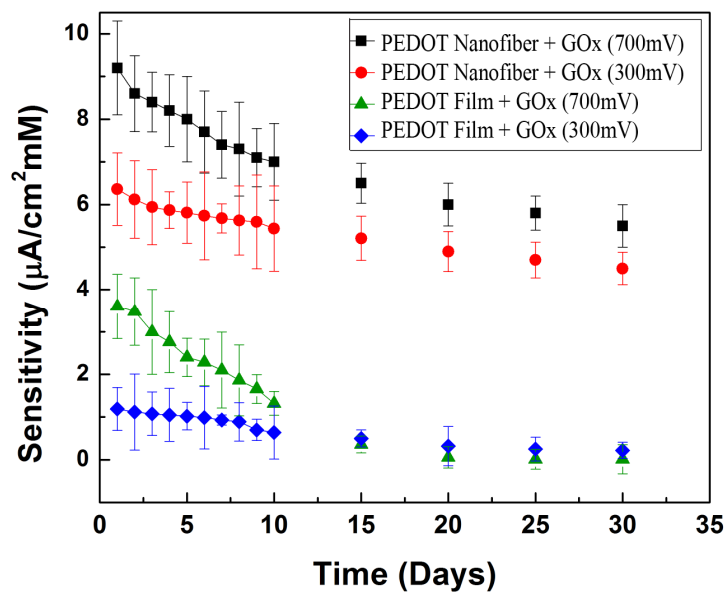


**Figure 15.** Sensitivity of PEDOT film + GOx and PEDOT nanofiber + GOx sensors at +300 mV and + 700mV over the course of 30 days.

The small loss in sensitivity in the PEDOT nanofiber + GOx sensors could be due either to better retention of the GOx enzyme and/or less loss of electroactivity over time than in the PEDOT film + GOx sensors. Since the sensitivity decrease that was observed is dependent on the polarization potential that was applied, the cyclic voltammetry (CV) behavior of PEDOT film + GOx and PEDOT nanofiber + GOx potentiostated at +700 mV and +300 mV was investigated (**Figure 16**).

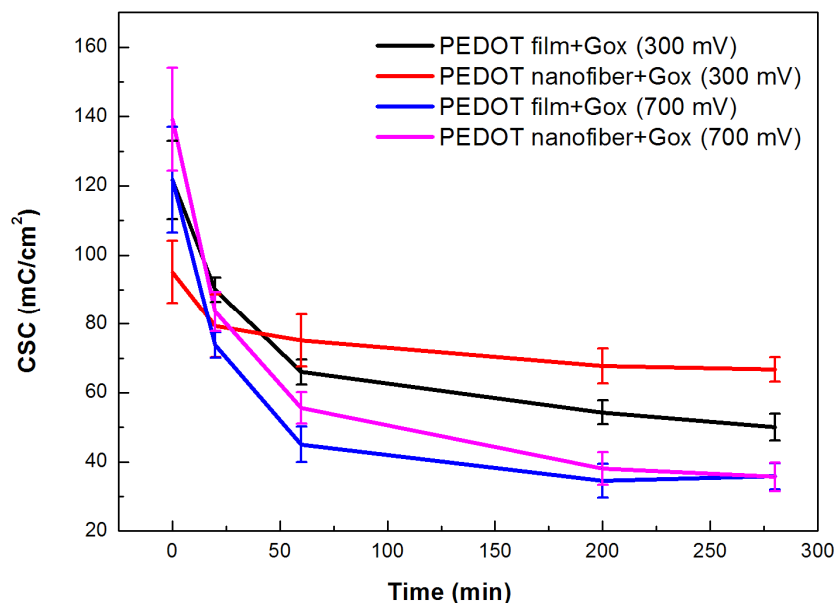


**Figure 16.** Charge storage capacity (CSC) of PEDOT film + GOx and PEDOT nanofiber + GOx at + 300mV and + 700 mV potential over 280 minutes of CV.

At 700 mV, the charge storage capacity (CSC) of PEDOT film + GOx at 280 min was  $35.8 \pm 3.8 \text{ mC/cm}^2$ , showing a 70.6% drop compared with the CSC at 0 min ( $121.8 \text{ m} \pm 15.2 \text{ mC/cm}^2$ ). For the PEDOT nanofiber group, the CSC at 280 min was  $35.6 \pm 4.1 \text{ mC/cm}^2$ , indicating a 74.4% drop compared with the CSC at 0 min ( $139.2 \pm 14.8 \text{ mC/cm}^2$ ). At 300 mV, the PEDOT film + GOx group has CSC value of  $50.0 \pm 3.9 \text{ mC/cm}^2$ , showing 58.9% decrease compared with the CSC at 0 min ( $121.6 \pm 11.3 \text{ mC/cm}^2$ ). For the PEDOT nanofiber + GOx group, the CSC at 280 min was  $66.8 \pm 3.6 \text{ mC/cm}^2$ , indicating 29.8% decrease compared with the CSC at 0 min ( $95.1 \pm 9.1 \text{ mC/cm}^2$ ). These results are in accordance with the loss of sensitivity study above and demonstrate that +700 mV groups lead to more electroactivity loss than +300 mV groups. It should also be noted that the CV curves for the PEDOT film (nanofiber) without GOx were slightly different from those of the PEDOT film (nanofiber) + GOx. The anodic peak at around -0.78 V was broadened and cathodic peak at around -0.50 V appeared when GOx was incorporated. This result may be due to the interaction between GOx and PEDOT during potential sweeping.

## 2.3 Conclusion

This work demonstrates the potential benefits of nanostructured conducting polymer biosensors, including reduced impedance and increased entrapment of bioactive molecules per electrode surface area resulting in increased sensitivity and lower limits of detections.

Additionally, nanostructured conducting polymer biosensors showed improved stability compared to films, which was evidenced by less loss of sensitivity over time due to a smaller loss of charge storage capacity. Use of low polarization potentials further enhanced this effect. This work also serves as a proof of concept of the advantage of using such sensor designs and can serve as a model for sensors designed for the detection of other neurochemicals and neurotransmitters.

## **Chapter 3. CONDUCTING POLYMER – HYDROGEL NANOFIBERS**

The previous chapter demonstrated the potential benefits of nanostructured conducting polymer biosensors, including reduced impedance and increased entrapment of bioactive molecules per electrode surface area resulting in increased sensitivity and lower limits of detections, as well as improved stability compared to conducting polymer films. However, the sensor fabrication relies on the use of traditional metal substrates, which are hard, dry, and static compared to biological tissue. Additionally, while conducting polymers have mechanical properties more similar to biological soft tissue than metals do, they are not soft and flexible as many other polymeric materials such as hydrogels. Therefore, it has been suggested that copolymers of hydrogels and conducting polymers could better meet the needs of a neural interface material (Green, Baek et al. 2010).

The differences in mechanical properties between the implanted device and the tissue can be of critical importance. For example, within the nervous system, stiff substrates (over 300 Pa) lead to significant  $\text{Ca}^{+2}$  influx correlating to adhesion site detachment, neurite retraction, and a reduction in neurite branches (Franze and Guck 2010). Also, it has been demonstrated that regenerating axons extend more rapidly on compliant substrates with mechanical properties more similar to native tissue (Sundararaghavan, Monteiro et al. 2009).

Therefore, the second part of this thesis describes the fabrication of conductive hydrogel copolymers with the aim of fabricating soft, conductive nanofibers without the use of metal substrates. Several types of conductive nanofibers have been electrospun from combinations of conductive polyaniline or polypyrrole with other polymers, such as polymethylmethacrylate (Veluru, Satheesh et al. 2007), polylactic acid (Prabhakaran, Ghasemi-Mobarakeh et al. 2011), polyethylene oxide (Norris, Shaker et al. 2000), and polycaprolactone. Two such nanofiber mats were used as scaffolds for cardiomyocytes (Kai, Prabhakaran et al. 2011) and for nerve cells, which led to improved neurite outgrowth (Prabhakaran, Ghasemi-Mobarakeh et al. 2011). While these studies show the feasibility of producing nanofibers from blends of conducting polymer and non-conductive co-polymer, these examples used organic solvents, which create challenges for incorporation of water-soluble biomolecules.

PEDOT:PSS nanoparticles dispersed in water are highly conductive and stable and such a dispersion is commercially available. The ability to mix these PEDOT:PSS nanoparticles with other water-soluble materials to create novel hybrids with conductive properties has

been demonstrated. PEDOT:PSS nanoparticles have been combined with latex to form an elastomeric and flexible conductive material (Yin, Wu et al. 2012), with polyethylene oxide to form an actuator (Ikushima, John et al. 2010), and with poly(vinyl alcohol) – poly(acrylic acid) interpenetrating network to create an optrode (Lu, Li et al. 2012).

PEDOT:PSS nanoparticle dispersion cannot be electrospun into nanofibers due to its low inherent viscosity; however, nanofibers containing PEDOT:PSS nanoparticles have been created by using PEO as a co- polymer to enable electrospinning. This combination is feasible because both polymers are water-soluble, and such a combination could allow for future incorporation of water-soluble biomolecules (Bedford, Winget et al. 2011). The aim here is to characterize the fabrication of PEDOT:PSS – PEO copolymer fibers and quantify the electrical properties of such fibers.

### 3.1 Materials & Methods

Polyethyene oxide (PEO) (M.W. 900,000), pentaerythritol triacrylate (PETA), and 2.2% PEDOT:PSS nanoparticles dispersed in water were purchased from Sigma. All chemicals were used as received to prepare aqueous solutions containing 4 wt% polyethylene oxide, 0.4 wt% PETA, and PEDOT:PSS nanoparticles. Solutions were stirred overnight prior to use, and were designated by their PEDOT:PSS content with percentages ranging from 0% to 25% of total polymer weight.

Conducting polymer- hydrogel films were fabricated by casting solutions containing 0%, 15%, 20%, or 25% PEDOT:PSS onto substrates. The films were subsequently crosslinked using 345 nm UV light with an intensity of  $4800 \mu\text{W cm}^{-2}$  for 30 minutes. The feasibility of crosslinking PEO with UV radicalized PETA has previously been demonstrated (Zhou, Wang et al. 2012).

Similarly, nanofibers were electrospun from solutions containing 0%, 15%, 20%, or 25% PEDOT:PSS; fibers with a PEDOT:PSS content above 25% PEDOT:PSS could not be electrospun. A flow rate of  $500 \text{ uL hr}^{-1}$  and a potential of 15 kV at a distance of 20 cm from the target was used for all solutions, except those with 25% PEDOT:PSS, which required a 10 kV potential. After electrospinning, the fibers were crosslinked as above. It is possible that the 25% PEDOT:PSS required a lower potential due to the higher electrical conductivity of the polymer solution (Greiner and Wendorff 2007). It has been shown that as the electrical field is raised above a certain threshold, the polymer jet moves back to the edge of the metal

needle, eliminating the polymer drop and the Taylor cone needed for electrospinning (Pham, Sharma et al. 2006).

Scanning electron microscopy (SEM) was used to measure the PEDOT:PSS – PEO fiber diameters and observe fiber morphology. Samples were sputter coated with a thin layer of gold prior to imaging, and diameters were measured for fibers with 0%, 15%, 20%, or 25% PEDOT:PSS content. Transmission electron microscopy with energy dispersive spectroscopy (TEM/EDS) was used to verify the incorporation of PEDOT:PSS into the nanofibers by detecting the presence of sulfur in the fibers. TEM/EDS was performed on fibers with 0% or 25% PEDOT:PSS.

To measure swelling ratios, PEDOT:PSS – PEO films and PEDOT:PSS – PEO nanofibers with 0%, 15%, 20%, and 25% PEDOT:PSS content were fabricated on aluminum foil substrates. Samples were swollen in distilled water at room temperature for six hours. They were then removed from the water, and excess water was carefully blotted off the sample. Samples were weighed in this swollen state prior to drying them in an oven at 150 °F for 30 minutes. The dried samples were then weighed, and the swelling ratio was calculated as the ratio of swollen weight of the sample to dried weight of the sample.

Finally, the impedance spectroscopy of the PEDOT:PSS – PEO films and PEDOT:PSS – PEO nanofibers with 0%, 15%, 20%, and 25% PEDOT:PSS content were measured. Samples were prepared on gold electrodes. Impedance spectroscopy was measured for samples immersed in PBS while frequencies were swept from 100 kHz to 0.1 Hz using a 0.01 V sine wave. The impedance of the bare gold electrodes was measured prior to sample preparation, and the percent change in impedance after application of the films or nanofibers to the electrodes was calculated at a frequency of 10 Hz.

### 3.2 Results & Discussion

SEM showed that PEDOT:PSS – PEO nanofibers fabricated using identical spinning conditions (0%, 15%, and 20% PEDOT:PSS) had uniform morphologies (**Figure 17**) and statistically similar diameters ( $p < 0.05$ ) (**Figure 18**). The diameters of these fibers were in the 220 – 300 nm range, which is consistent with previous reports of PEO nanofibers using water as a solvent. (Son, Youk et al. 2004) The fibers containing 25% PEDOT:PSS had diameters of  $435 \pm 34$  nm, which is statistically larger diameters than the other samples ( $p < 0.05$ ); however, these 25% PEDOT:PSS fibers were fabricated from a more viscous solution and

with a lower electric field strength, and both of these factors have been shown to increase fiber diameter (Li and Xia 2004).

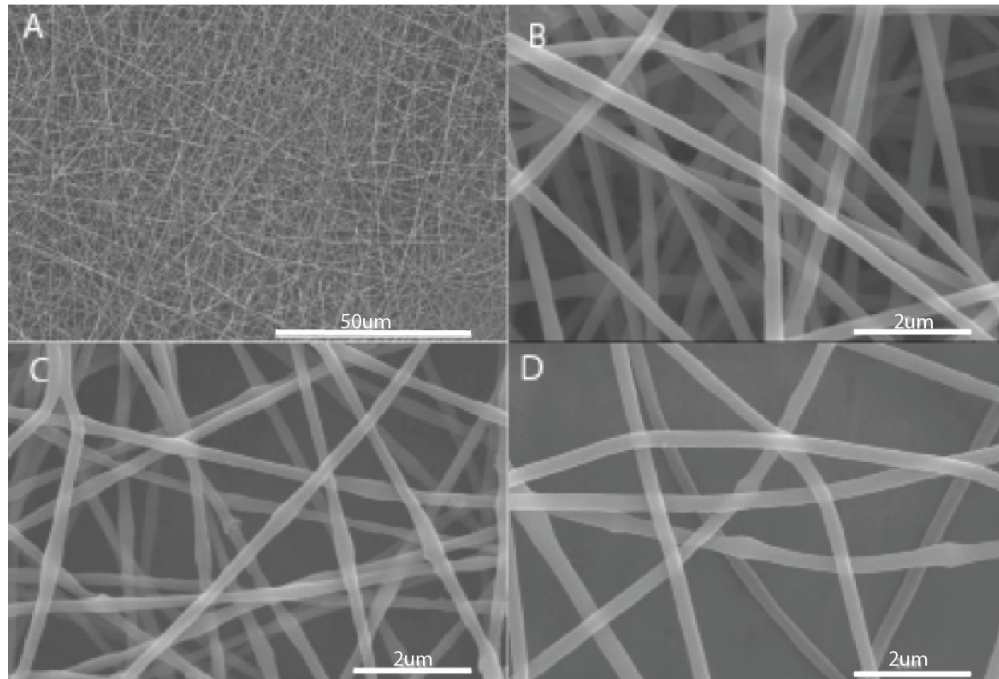


**Figure 17.** SEM images of electrospun nanofibers of 0% PEDOT:PSS - PEO (B), 15% PEDOT:PSS - PEO (A,C), and 25% PEDOT:PSS - PEO (D) showing randomly oriented mats of nanofibers and similar nanofiber morphology for each PEDOT:PSS concentration. 20% PEDOT:PSS- PEO nanofibers had similar morphology (not shown).

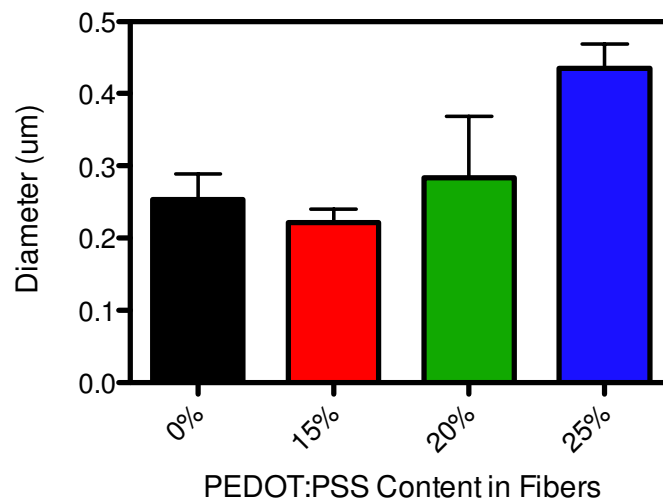


**Figure 18.** Diameter of PEDOT:PSS-PEO nanofibers by PEDOT:PSS content.

Transmission electron microscopy with energy dispersive spectroscopy (TEM/EDS) was used to verify the incorporation of PEDOT:PSS into the nanofibers. These spectra indicate the presence of sulfur in the fibers containing PEDOT:PSS, which is not seen in the spectra for the 0% PEDOT:PSS - PEO fibers (**Figure 19**). This analysis confirms the presence of the PEDOT:PSS nanoparticles within the electrospun nanofibers, as sulfur increases from 0.05 atomic % to 11.85 atomic % when 25% PEDOT:PSS is added to the solution. The peaks identified as Cu are artifacts of the TEM grid used.

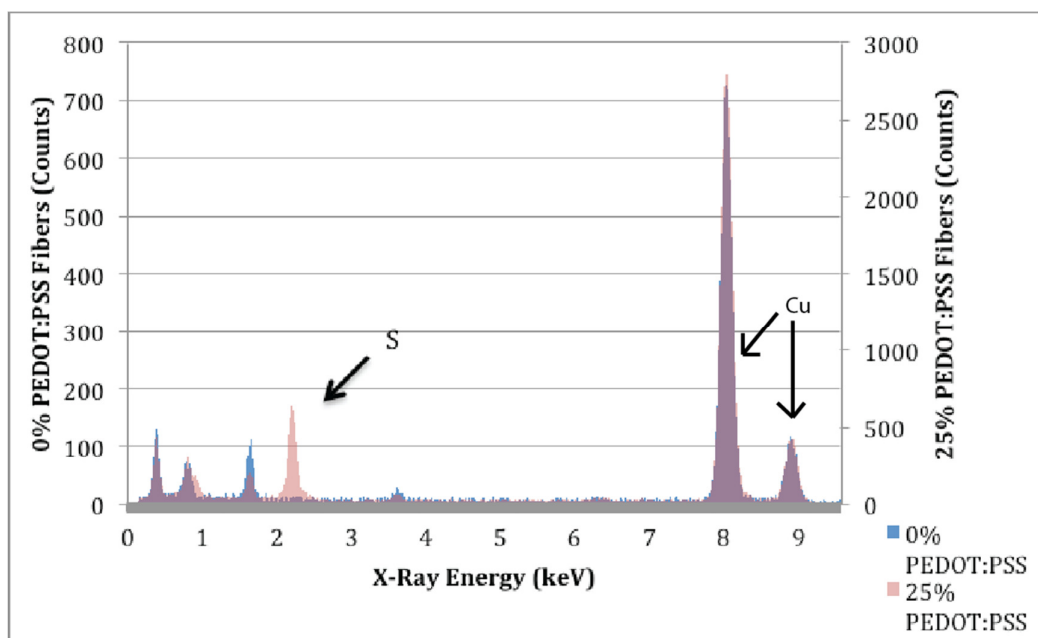


**Figure 19.** EDS spectra obtained for a mat of PEDOT:PSS - PEO nanofibers fabricated from a solution containing 0% PEDOT:PSS or 25% PEDOT:PSS. The sulfur peak indicates the presence of PEDOT:PSS nanoparticles within the 25% PEDOT:PSS nanofibers that is absent in the 0% PEDOT:PSS nanofibers.

The swelling ratio of PEDOT:PSS – PEO films and nanofibers was measured. Increasing amounts of PEDOT:PSS within the samples led to a decreasing trend in swelling ratio (**Table 1**). Films with 25% PEDOT:PSS swelled  $16 \pm 3$  times, which was significantly less than those with 0% PEDOT:PSS ( $p < 0.05$ ). Fibers with 25% PEDOT:PSS swelled  $36 \pm 7$  times, which was also significantly less than those with 0% PEDOT:PSS ( $p < 0.05$ ). The hydrophobic nature of PEDOT may have prevented as much water from entering the bulk of the material during swelling, thereby decreasing the swelling ratio in samples with higher PEDOT:PSS content.

PEDOT:PSS content	Swelling Ratio	
	Films	Nanofibers
0%	78 ± 16	52 ± 9
15%	67 ± 16	41 ± 4
20%	49 ± 8	37 ± 8
25%	16 ± 3	36 ± 7

**Table 1.** Swelling ratio of PEDOT:PSS - PEO films and nanofibers made from solutions containing 0%, 15%, 20%, or 25% PEDOT:PSS.

Next, the electrical characteristics of the PEDOT:PSS – PEO films and PEDOT:PSS – PEO nanofibers with 0%, 15%, 20%, and 25% PEDOT:PSS content were measured. The 0% PEDOT:PSS-PEO samples increased the impedance compared to the bare gold electrodes as would be expected from applying a non-conductive coating to the electrode; the 0% PEDOT:PSS - PEO films increased impedance at 10 Hz by  $159 \pm 63\%$  compared to  $31 \pm 26\%$  for the 0% PEDOT:PSS – PEO nanofibers. This difference could be explained by a more complete coverage of the gold electrode by the film, whereas the porous nanofiber mat could have gaps in its contact with the electrode thereby allowing some areas of the electrode to be exposed directly to the solution.

The film and nanofiber samples containing 15% PEDOT:PSS, 20% PEDOT:PSS, and 25% PEDOT:PSS decreased the impedance compared to the bare gold electrodes, and the samples with higher PEDOT:PSS content exhibited greater reduction in impedance (**Figure 20**). 15% PEDOT:PSS films showed a  $48.44 \pm 12.07\%$  reduction compared to  $83.37 \pm 9.33\%$  reduction for 25% PEDOT:PSS films; 15% PEDOT:PSS nanofibers showed a  $48.15 \pm 28.80\%$  reduction compared to  $87.19 \pm 14.99\%$  for 25% PEDOT:PSS nanofibers. Statistical 2-way ANOVA for this data indicates that PEDOT:PSS content statistically affects the change in impedance ( $p < 0.0003$ ) while sample morphology (films compared to nanofibers) does not affect the change in impedance at a single frequency of 10 Hz.

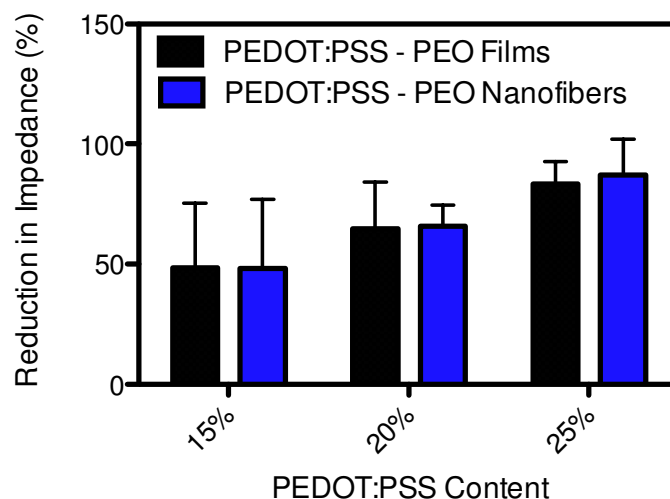


**Figure 20.** Reduction in impedance at 10 Hz in PEDOT:PSS – PEO film and PEDOT:PSS – PEO nanofiber samples.

Individual crosslinked PEDOT:PSS – PEO nanofibers maintained their morphology when immersed in water and dried; however, the nanofiber mats had large swelling ratios. When emerged in aqueous solution, such as during impedance spectroscopy, the fibers swelled and some merged together rather than maintained their distinct morphology. This effect could explain the similarity in impedance changes seen for PEDOT:PSS – PEO film and PEDOT:PSS – PEO nanofibers and suggests that an improved crosslinking method is needed to reduce the swelling ratio of the material.

It is predicted that the impedance of a conductive PEDOT:PSS – PEO nanofiber mat should be less than that of a similar film due to an increase in effective surface area when using the nanofiber mat. In previous studies on the conductivity of blended polymer films and nanofibers containing a conductive polymer, a four-point probe method was used in which the samples were dry rather than immersed in aqueous solution. In that arrangement, the films had higher conductivity than the corresponding nanofiber mats. The authors attributed this result to the fact that the ‘fill factor’ for the porous nanofiber mats is much less than the films, but asserted that the conductivity of an individual fiber should be approximately equal to that of the film (Norris, Shaker et al. 2000).

While the PEDOT:PSS – PEO films and PEDOT:PSS - PEO nanofibers in this study had similar effects on electrode impedance at 10 Hz, the impedance spectra over the full 100 kHz to 0.1 Hz range were different for PEDOT:PSS - PEO films compared to PEDOT:PSS – PEO nanofibers (**Figure 21**). Although the PEDOT:PSS – PEO nanofibers resulted in a general downwards shift of the bare gold impedance curve at frequencies less than 1 kHz, the

PEDOT:PSS – PEO films had a distinctly different response. It is possible that the PEDOT:PSS – PEO nanofibers did not adhere well to the gold electrodes, and therefore, while the increased surface area resulted in a shift downwards in impedance, the full extent of the electrical properties of the PEDOT:PSS – PEO nanofibers was not captured. For the PEDOT:PSS – PEO films, at low frequencies, they have lower impedance and are more resistive than the bare gold or PEDOT:PSS – PEO nanofibers as demonstrated by the flat impedance across a range of frequencies; however, at high frequencies, the material more closely follows that of the bare gold electrode.

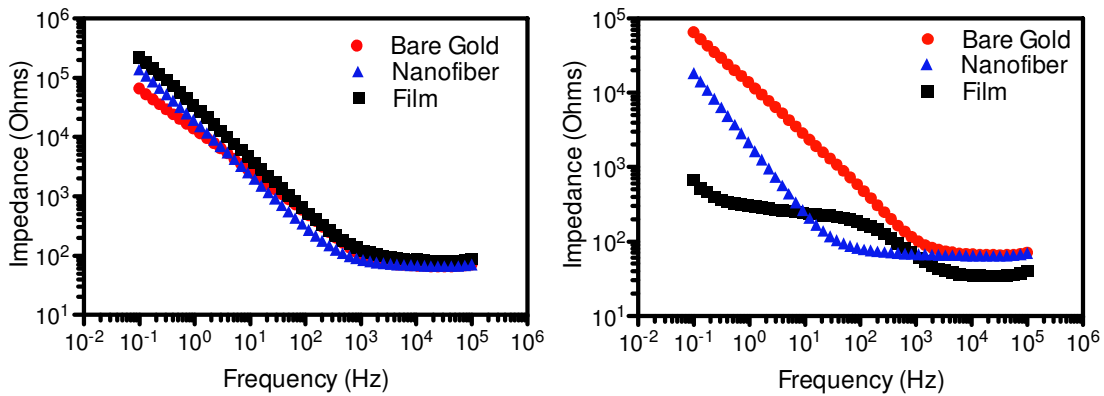


**Figure 21.** Impedance spectra for 0% PEDOT:PSS – PEO samples (A) and 25% PEDOT:PSS – PEO samples (B).

### 3.3 Conclusion

This work confirmed previous findings that blends of PEDOT:PSS nanoparticles with PEO can be electrospun to form conductive, hydrogel nanofibers (Bedford, Winget et al. 2011). The inclusion of increasing amounts of PEDOT:PSS nanoparticles was shown to decrease the swelling ratio of the blended material. Both PEDOT:PSS – PEO film and nanofibers reduced the impedance of gold electrodes coated with these materials. Future studies could further characterize such materials by measuring mechanical properties, electrical stability over time, or biocompatibility. Applications such as biosensing, actuated release of biomolecules, or stimulation of axonal regeneration could also be explored. Such conductive hydrogel nanofibers could find potential use in the field of soft electronics or tissue engineering.

## Chapter 4. CONCLUSION & FUTURE DIRECTION

This thesis explores two neural interface materials consisting of conductive nanofibers. The first material is conducting polymer nanofibers that incorporate glucose oxidase. This material was designed to be used at the recording site of a glucose biosensor. The conducting polymer nanofibers provided increased sensitivity, decreased limits of detection, and improved longevity in the sensors compared to similar films. It was also demonstrated that use of lower polarization potentials during sensing increased the longevity of the sensors. While the experiments indicate that the conducting polymer nanofiber sensors incorporate significantly more glucose oxidase than similar film sensors, the number of samples in this investigation was limited. Better quantification of the amount of enzyme in each type of sensor could distinguish how much of the increase in sensitivity recorded in the nanofibers is due to increased enzyme incorporation and how much is due to reduced impedance.

Future studies with these conducting polymer nanofiber sensors could explore the loss of enzyme from the sensors due to leaching over time, the sensitivity reduction over a period of time longer than 30 days, and the interference of other biomolecules in the detection of glucose. Additionally, these conducting polymer nanofiber sensors serve as a proof-of-concept to be used for the detection of other neurochemicals such as neurotransmitters.

The second material is conducting polymer – hydrogel copolymer nanofibers. The incorporation of the hydrogel copolymer allowed for the electrospinning of conducting polymer. Incorporation of higher percentages of conducting polymer nanoparticles led to reduced swelling and reduced impedance of the nanofibers. Some loss of morphology was seen in the nanofibers after prolonged immersion in aqueous solution, and an improved method of crosslinking is needed. Additionally, the gold electrodes used in this study lacked repeatability in their impedance, thereby requiring a change in impedance to be measured for each sample. Measurements of absolute impedance for the conducting polymer – hydrogel copolymer nanofibers would be desirable and comparisons at the biologically relevant 1kHz frequency could provide some additional perspective on the benefits of using such a material *in vivo*.

Future studies with this conducting polymer – hydrogel copolymer nanofibers should examine the mechanical properties and address how these soft materials could be inserted into the body with minimal tissue damage. The use of such materials to incorporate and release biomolecules should be evaluated and eventually an analysis of the material's biocompatibility and usefulness as a neural regeneration scaffold should be gauged.

## Bibliography

- Abidian, M. R., J. M. Corey, et al. (2010). "Conducting-Polymer Nanotubes Improve Electrical Properties, Mechanical Adhesion, Neural Attachment, and Neurite Outgrowth of Neural Electrodes." Small **6**(3): 421-429.
- Abidian, M. R., E. D. Daneshvar, et al. (2012). "Hybrid Conducting Polymer-Hydrogel Conduits for Axonal Growth and Neural Tissue Engineering." Advanced Healthcare Materials **1**(6): 762-767.
- Abidian, M. R., D. H. Kim, et al. (2006). "Conducting-polymer nanotubes for controlled drug release." Advanced Materials **18**(4): 405-+.
- Abidian, M. R., K. A. Ludwig, et al. (2009). "Interfacing Conducting Polymer Nanotubes with the Central Nervous System: Chronic Neural Recording using Poly (3,4-ethylenedioxythiophene) Nanotubes." Advanced Materials **21**(37): 3764-3770.
- Adams, R. N. (1976). "Probing Brain Chemistry with Electroanalytical Techniques " Analytical Chemistry **48**(14): 1126-&.
- Ahuja, T., I. A. Mir, et al. (2007). "Biomolecular immobilization on conducting polymers for biosensing applications." Biomaterials **28**(5): 791-805.
- Balasubramanian, K. (2010). "Challenges in the use of 1D nanostructures for on-chip biosensing and diagnostics: A review." Biosensors & Bioelectronics **26**(4): 1195-1204.
- Bedford, N. M., G. D. Winget, et al. (2011). "Immobilization of Stable Thylakoid Vesicles in Conductive Nanofibers by Electrospinning." Biomacromolecules **12**(3): 778-784.
- Belanger, D., J. Nadreau, et al. (1989). "Electrochemistry of the polypyrrole glucose oxidase electrode." Journal of Electroanalytical Chemistry **274**: 143-155.
- Burdette, S. C. and S. J. Lippard (2003). "Meeting of the minds: Metalloneurochemistry." Proceedings of the National Academy of Sciences of the United States of America **100**(7): 3605-3610.
- Cogan, S. F. (2008). Neural stimulation and recording electrodes. Annual Review of Biomedical Engineering. Palo Alto, Annual Reviews. **10**: 275-309.
- De Fazio, M., R. Rammo, et al. (2011). "Alterations in Cerebral Oxidative Metabolism following Traumatic Brain Injury." Neurocritical Care **14**(1): 91-96.
- Dodla, M. C. and R. V. Bellamkonda (2008). "Differences between the effect of anisotropic and isotropic laminin and nerve growth factor presenting scaffolds on nerve regeneration across long peripheral nerve gaps." Biomaterials **29**(1): 33-46.

- Fattahi, P., G. Yang, et al. (2014). "A Review of Organic and Inorganic Biomaterials for Neural Interfaces." Advanced Materials **26**(12): 1846-1885.
- Fortier, G. and D. Belanger (1991). "Characterization of the Biochemical Behavior of Glucose-Oxidase Entrapped in a Polypyrrole Film " Biotechnology and Bioengineering **37**(9): 854-858.
- Franze, K. and J. Guck (2010). "The biophysics of neuronal growth." Reports on Progress in Physics **73**(9).
- Gerard, M., A. Chaubey, et al. (2002). "Application of conducting polymers to biosensors." Biosensors & Bioelectronics **17**(5): 345-359.
- Gomez, N., J. Y. Lee, et al. (2007). "Micropatterned polypyrrole: A combination of electrical and topographical characteristics for the stimulation of cells." Advanced Functional Materials **17**(10): 1645-1653.
- Green, R. A., S. Baek, et al. (2010). "Conducting polymer-hydrogels for medical electrode applications." Science and Technology of Advanced Materials **11**(1).
- Green, R. A., N. H. Lovell, et al. (2008). "Conducting polymers for neural interfaces: Challenges in developing an effective long-term implant." Biomaterials **29**(24-25): 3393-3399.
- Greiner, A. and J. H. Wendorff (2007). "Electrospinning: A fascinating method for the preparation of ultrathin fibres." Angewandte Chemie-International Edition **46**(30): 5670-5703.
- Groenendaal, B. L., F. Jonas, et al. (2000). "Poly(3,4-ethylenedioxythiophene) and its derivatives: Past, present, and future." Advanced Materials **12**(7): 481-494.
- Groenendaal, L., G. Zotti, et al. (2003). "Electrochemistry of poly(3,4-alkylenedioxythiophene) derivatives." Advanced Materials **15**(11): 855-879.
- Guimard, N. K., N. Gomez, et al. (2007). "Conducting polymers in biomedical engineering." Progress in Polymer Science **32**(8-9): 876-921.
- Gurunathan, K., A. V. Murugan, et al. (1999). "Electrochemically synthesised conducting polymeric materials for applications towards technology in electronics, optoelectronics and energy storage devices." Materials Chemistry and Physics **61**(3): 173-191.
- Hinberg, I., A. Kapoulas, et al. (1974). "Gel Entrapment of Enzymes - Kinetic Studies of Immobilized Glucose Oxidase." Biotechnology and Bioengineering **16**(2): 159-168.
- Hochberg, L. R., D. Bacher, et al. (2012). "Reach and grasp by people with tetraplegia using a neurally controlled robotic arm." Nature **485**(7398): 372-U121.

- Hoffman-Kim, D., J. A. Mitchel, et al. (2010). Topography, Cell Response, and Nerve Regeneration. Annual Review of Biomedical Engineering, Vol 12. M. L. Yarmush, J. S. Duncan and M. L. Gray. Palo Alto, Annual Reviews. **12**: 203-231.
- Hurtado, A., J. M. Cregg, et al. (2011). "Robust CNS regeneration after complete spinal cord transection using aligned poly-L-lactic acid microfibers." Biomaterials **32**(26): 6068-6079.
- Ikushima, K., S. John, et al. (2010). "PEDOT/PSS bending actuators for autofocus micro lens applications." Synthetic Metals **160**(17-18): 1877-1883.
- Kai, D., M. P. Prabhakaran, et al. (2011). "Polypyrrole-contained electrospun conductive nanofibrous membranes for cardiac tissue engineering." Journal of Biomedical Materials Research Part A **99A**(3): 376-385.
- Karumbaiah, L., T. Saxena, et al. (2013). "Relationship between intracortical electrode design and chronic recording function." Biomaterials **34**(33): 8061-8074.
- Kim, Y. T., J. M. Caldwell, et al. (2009). "Nanoparticle-mediated local delivery of methylprednisolone after spinal cord injury." Biomaterials **30**(13): 2582-2590.
- Koopal, C. G. J., M. C. Feiters, et al. (1992). "Glucose Sensor Utilizing Polypyrrole Incorporated in Track-Etch Membranes as the Mediator " Biosensors & Bioelectronics **7**(7): 461-471.
- Kros, A., R. J. M. Nolte, et al. (2002). "Poly (3,4-ethylenedioxythiophene)-based copolymers for biosensor applications." Journal of Polymer Science Part a-Polymer Chemistry **40**(6): 738-747.
- Kros, A., N. Sommerdijk, et al. (2005). "Poly(pyrrole) versus poly (3,4-ethylenedioxythiophene): implications for biosensor applications." Sensors and Actuators B-Chemical **106**(1): 289-295.
- Li, C. K. N. (1982). "The Glucose Distribution in 9L Rat-Brain Multicell Tumor Spheroids and Its Effect on Cell Necrosis " Cancer **50**(10): 2066-2073.
- Li, D. and Y. N. Xia (2004). "Electrospinning of nanofibers: Reinventing the wheel?" Advanced Materials **16**(14): 1151-1170.
- Lu, Y., Y. L. Li, et al. (2012). "Poly(3,4-ethylenedioxythiophene)/poly(styrenesulfonate)-poly(vinyl alcohol)/poly(acrylic acid) interpenetrating polymer networks for improving optrode-neural tissue interface in optogenetics." Biomaterials **33**(2): 378-394.

- Ludwig, K. A., J. D. Uram, et al. (2006). "Chronic neural recordings using silicon microelectrode arrays electrochemically deposited with a poly(3,4-ethylenedioxythiophene) (PEDOT) film." Journal of Neural Engineering **3**(1): 59-70.
- Lundin, V., A. Herland, et al. (2011). "Control of Neural Stem Cell Survival by Electroactive Polymer Substrates." Plos One **6**(4).
- MacDiarmid, A. G. (2001). "Synthetic metals: a novel role for organic polymers." Synthetic Metals **125**(1): 11-22.
- Medicine, U. S. N. L. o. (2014). A.D.A.M. Medical Encyclopedia. U. S. D. o. H. a. H. Services. Bethesda, MD.
- Namba, H., Y. Iwadate, et al. (1998). "Glucose and methionine uptake by rat brain tumor treated with prodrug-activated gene therapy." Nuclear Medicine and Biology **25**(3): 247-250.
- Nien, P. C., T. S. Tung, et al. (2006). "Amperometric glucose biosensor based on entrapment of glucose oxidase in a poly(3,4-ethylenedioxythiophene) film." Electroanalysis **18**(13-14): 1408-1415.
- Norris, I. D., M. M. Shaker, et al. (2000). "Electrostatic fabrication of ultrafine conducting fibers: polyaniline/polyethylene oxide blends." Synthetic Metals **114**(2): 109-114.
- Park, K. I., Y. D. Teng, et al. (2002). "The injured brain interacts reciprocally with neural stem cells supported by scaffolds to reconstitute lost tissue." Nature Biotechnology **20**(11): 1111-1117.
- Pham, Q. P., U. Sharma, et al. (2006). "Electrospinning of polymeric nanofibers for tissue engineering applications: A review." Tissue Engineering **12**(5): 1197-1211.
- Piro, B., L. A. Dang, et al. (2001). "A glucose biosensor based on modified-enzyme incorporated within electropolymerised poly(3,4-ethylenedioxythiophene) (PEDT) films." Journal of Electroanalytical Chemistry **512**(1-2): 101-109.
- Prabhakaran, M. P., L. Ghasemi-Mobarakeh, et al. (2011). "Electrospun conducting polymer nanofibers and electrical stimulation of nerve stem cells." Journal of Bioscience and Bioengineering **112**(5): 501-507.
- Prevention, C. f. D. C. a. (2011). National Diabetes Factsheet. U. S. D. o. H. H. Services. Atlanta.
- Ramanavicius, A., A. Ramanaviciene, et al. (2006). "Electrochemical sensors based on conducting polymer- polypyrrole." Electrochimica Acta **51**(27): 6025-6037.
- Robinson, D. A. (1968). "Electrical Properties of Metal Microelectrodes " Proceedings of the Institute of Electrical and Electronics Engineers **56**(6): 1065-&.

- Runge, M. B., M. Dadsetan, et al. (2010). "Development of Electrically Conductive Oligo(polyethylene glycol) Fumarate-Polypyrrole Hydrogels for Nerve Regeneration." Biomacromolecules **11**(11): 2845-2853.
- Sangodkar, H., S. Sukeerthi, et al. (1996). "A biosensor array based on polyaniline." Analytical Chemistry **68**(5): 779-783.
- Schmidt, C. E. and J. B. Leach (2003). "Neural tissue engineering: Strategies for repair and regeneration." Annual Review of Biomedical Engineering **5**: 293-347.
- Sekine, S., Y. Ido, et al. (2010). "Conducting Polymer Electrodes Printed on Hydrogel." Journal of the American Chemical Society **132**(38): 13174-13175.
- Shaolin, M., X. Huaiguo, et al. (1991). "Bioelectrochemical responses of the polyaniline glucose oxidase electrode." Journal of electroanalytical chemistry and interfacial electrochemistry **304**(1): 7-16.
- Silva, G. A. (2006). "Neuroscience nanotechnology: Progress, opportunities and challenges." Nature Reviews Neuroscience **7**(1): 65-74.
- Silver, J. and J. H. Miller (2004). "Regeneration beyond the glial scar." Nature Reviews Neuroscience **5**(2): 146-156.
- Smela, E. (2003). "Conjugated polymer actuators for biomedical applications." Advanced Materials **15**(6): 481-494.
- Smela, E. (2008). "Conjugated polymer actuators." Mrs Bulletin **33**(3): 197-204.
- Son, W. K., J. H. Youk, et al. (2004). "The effects of solution properties and polyelectrolyte on electrospinning of ultrafine poly(ethylene oxide) fibers." Polymer **45**(9): 2959-2966.
- Sundararaghavan, H. G., G. A. Monteiro, et al. (2009). "Neurite Growth in 3D Collagen Gels With Gradients of Mechanical Properties." Biotechnology and Bioengineering **102**(2): 632-643.
- Szarowski, D. H., M. D. Andersen, et al. (2003). "Brain responses to micro-machined silicon devices." Brain Research **983**(1-2): 23-35.
- Veluru, J. B., K. K. Satheesh, et al. (2007). "Electrical Properties of Electrospun Fibers of PANI-PMMA Composites." Journal of Engineered Fibers and Fabrics **2**(2): 25-31.
- Wallace, G. G., M. Smyth, et al. (1999). "Conducting electroactive polymer-based biosensors." Trac-Trends in Analytical Chemistry **18**(4): 245-251.
- Wang, G. J., N. D. Volkow, et al. (1996). "Glucose metabolic changes in nontumoral brain tissue of patients with brain tumor following radiotherapy: A preliminary study." Journal of Computer Assisted Tomography **20**(5): 709-714.

- Wei, D., M. J. A. Bailey, et al. (2009). "Electrochemical biosensors at the nanoscale." Lab on a Chip **9**(15): 2123-2131.
- Wilson, G. S. and R. Gifford (2005). "Biosensors for real-time in vivo measurements " Biosensors & Bioelectronics **20**: 2388-2403.
- Yamato, H., M. Ohwa, et al. (1995). "Stability of Polypyrrole and Poly(3,4-ethylenedioxythiophene) for Biosensor Application." Journal of Electroanalytical Chemistry **397**(1-2): 163-170.
- Yin, H. E., C. H. Wu, et al. (2012). "Innovative elastic and flexible conductive PEDOT:PSS composite films prepared by introducing soft latexes." Journal of Materials Chemistry **22**(9): 3800-3810.
- Yiu, G. and Z. G. He (2006). "Glial inhibition of CNS axon regeneration." Nature Reviews Neuroscience **7**(8): 617-627.
- Zhou, C. J., Q. W. Wang, et al. (2012). "UV-initiated crosslinking of electrospun poly(ethylene oxide) nanofibers with pentaerythritol triacrylate: Effect of irradiation time and incorporated cellulose nanocrystals." Carbohydrate Polymers **87**(2): 1779-1786.